Czech technical university in Prague
Faculty of Nuclear Sciences and Physical Engineering

Department of solid state physics
Obor: Solid state physics

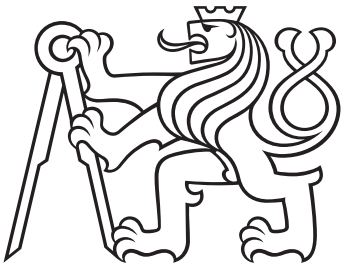

Study of preferred orientation of molluscs shells by diffraction methods

BACHELOR THESIS

Author: Leonard Valko
Supervisor: Monika Kučeráková
Year: 2022

ČESKÉ VYSOKÉ UČENÍ TECHNICKÉ V PRAZE
FAKULTA JADERNÁ A FYZIKÁLNĚ INŽENÝRSKÁ
Katedra inženýrství pevných látek

ZADÁNÍ BAKALÁŘSKÉ PRÁCE

Student: **Leonard Valko**

Studijní program: **Aplikace přírodních věd**

Obor: **Inženýrství pevných látek**

Akademický rok: **2020/2021**

Název práce: Studium přednostní orientace lastur mlžů pomocí difrakčních metod (česky)

Název práce: Study of preferred orientation of molluscs shells by diffraction methods (anglicky)

Pokyny pro vypracování:

Bakalářská práce je zaměřena na propojení difrakčních technik (zejména neutronové difrakce) se systémem vyhodnocovacích postupů při kvantitativní texturní analýze pomoci orientačně-distribuční funkce (ODF). Experimenty budou uskutečněny v laboratoři neutronové difrakce KIPL FJFI na difraktometru KSN-2 a na Oddělení strukturní analýzy FZU AV ČR na rentgenovém difraktometru SmartLab Rigaku. Zkoumanými vzorky budou lastury sladkovodních a mořských mlžů. Pro vyhodnocení a interpretaci experimentálních dat budou využity softwarové systémy GSAS, MTex (Matlab), Highscore (PANalytical), SmartStudio II (Rigaku) a Materiálové studio (Dessault Systems).

Při řešení postupujte podle následujících bodů.

I. Rešeršní/teoretická část
   1) Seznamte se s problematikou realizace experimentů pomocí difrakčních metod se zaměřením na studium textur.
   2) Seznamte se s procedurami pro vyhodnocení naměřených dat a systémem výpočtu orientačně distribuční funkce ODF.
   3) Vypracujte stručnou rešerši o současných poznatcích výzkumu lastur difrakčními metodami (zejména na důraz na neutronovou difrakci).

II. Experimentální část
   1) Na základě charakteristik difraktometru KSN-2 navrhněte uspořádání texturního experimentu s využitím goniometru HUBER pro orientaci měřených vzorků.
   2) Proveďte experimenty se vzorky lastur. Navrhněte instalaci těchto vzorků na jmenovaný goniometr.

3) Navrhněte a sestavte texturní experimenty zmíněných lasturních vzorků na rentgenovém difraktometru SmartLab Rigaku.
4) Získaná data zpracujte výše uvedenými postupy a programy. Výstupní údaje přehledně zpracujte a přehledně sestavte.
5) Dosažené výsledky porovnejte s údaji publikovanými v literatuře, uveďte význam vašich výsledků v rámci problematiky studia textur lastur a jim podobných materiálů.

Doporučená literatura:

[1] G.E. Bacon: Neutron Diffraction, 2nd. Ed., Oxford University Press, Oxford 1978.
[2] P.J. Young, R.S. Old, A.B. Free, et al.: J. Phys. Chem. **50** (2016) 346-351.
[3] D. Nikolayev, T. Lychagina, A. Pakhnevich: SN Applied Sciences **1** (2019) 344.
[4] J. Fryda, K. Klicnarova, B. Frydova, M. Mergl: Bulletin of Geosciences 85 (2010) 645-662.
[5] A. Checa: Tissue and Cell. **32** (2000) 405-416.
[6] D. Chateigner, C. Hedegaard , R. Wenk: Journal of Structural Geology **22** (2000) 1723-1735.

Jméno a pracoviště vedoucího práce:
Ing. Monika Kučeráková, Ph.D., Katedra inženýrství pevných látek, Fakulta jaderná fyzikálně inženýrská ČVUT v Praze

Jméno a pracoviště konzultanta:
prof. Ing. Stanislav Vratislav, CSc., Katedra inženýrství pevných látek, Fakulta jaderná fyzikálně inženýrská ČVUT v Praze

Datum zadání bakalářské práce: 26. 10. 2020

Termín odevzdání bakalářské práce: 7. 7. 2021

Doba platnosti zadání je dva roky od data zadání.

.....
garant

.....
vedoucí katedry

ČESKÉ VYSOKÉ UČENÍ TECHNICKÉ V PRAZE Fakulta jaderná a fyzikálně inženýrská -1-

.....
děkan

V Praze dne 26. 10. 2020

Declaration

I declare that this thesis is an original report of my research, has been written by me and has not been previously submitted, and that my research materials are listed in bibliography.

In Prague ....

Leonard Valko

Acknowledgements

First and foremost I am extremely grateful to my supervisor, Ing. Monika Kučeráková, Ph.D. and my consultant prof. Ing. Stanislav Vratislav, CSc. for their invaluable advice, continuous support, and patience during my bachelor study. Their immense knowledge and plentiful experience have encouraged me in all the time of my academic research and daily life.

Leonard Valko

Title:
Study of preferred orientation of molluscs shells by diffraction methods

Author:	Leonard Valko
Study programme :	Natural sciences application
Specialization:	Solid state physics
Type:	Bachelor thesis
Supervisor:	Monika Kučeráková Department of solid state physics, Faculty of Nuclear Sciences and Physical Engineering, Czech technical university in Prague
Consultant:	Stanislav Vratislav

Key words: molluscs, shells, diffraction, neutrons

Abstract: Aspect of this work was to convey the elementary theoretical knowledge about neutron physics and neutron diffraction. The experimental value of this work lies in determination of crystallographic structure of molluscs shells *Sinanodonta woodiana*. Among the findings of this work is confirmation of sharp maxima of the c-axis in pole figures (001) parallel to the inner surface of the shell. Findings of both neutron and X-ray diffraction supports this result. Another conclusion that was made was about rotation of a- and b-axis along the growth direction of the shell.

Contents

Chapter 1

Elementary information

1.1 Basics of crystallography

A crystal is an object made of atoms periodically arranged and distributed equidistantly in a spatial lattice. The abstract geometric arrangement is called a crystal lattice and defined as a series of nodes that represent positions of basis atoms in thermal equilibrium oscillating around the node. We speak about Bravais lattice when the arrangement of infinitely many atoms have all same neighborhood, orientated in a same way everywhere. Basis of crystal lattice is a set of specific atoms that occupy the locations of nodes provided by lattice. Basis may be composed of a single atom (commonly metals) or numerous atoms - molecules or polymers [8].

Unit cell is a parallelogram containing lattice nodes linked to the vertices of it. Unit cell may be defined by a translation vectors laid in edges $\vec{\boldsymbol{a}}, \vec{\boldsymbol{b}}, \vec{\boldsymbol{c}}$ of the parallelogram. We call the lengths a,b,c of these vectors and angles α, β, γ between them are called the lattice parameters. An unit cell that contains nodes only at its vertices is a primitive cell. More complex cells contain nodes in a face and space diagonals of unit cell. For describing a crystal we often need to talk about crystallographic planes of atoms, characterized by Miller indexes ***h, k, l***. The signature of crystallographic planes is written as ***(hkl)***. For more about the crystallography and Miller indexes, read [8].

Reciprocal lattice

In process of depicting crystal we employ and abstract reciprocal lattice. We construct this abstract space by attaching normals to the planes ***(hkl)*** and creating a points of reciprocal lattice at the distance of $\frac{1}{d_{hkl}}$ away from the plane on a normal vector [8]. d_{hkl} represents a distance between the planes ***h, k, l*** in direct lattice. Process can be seen in figure 1.1.

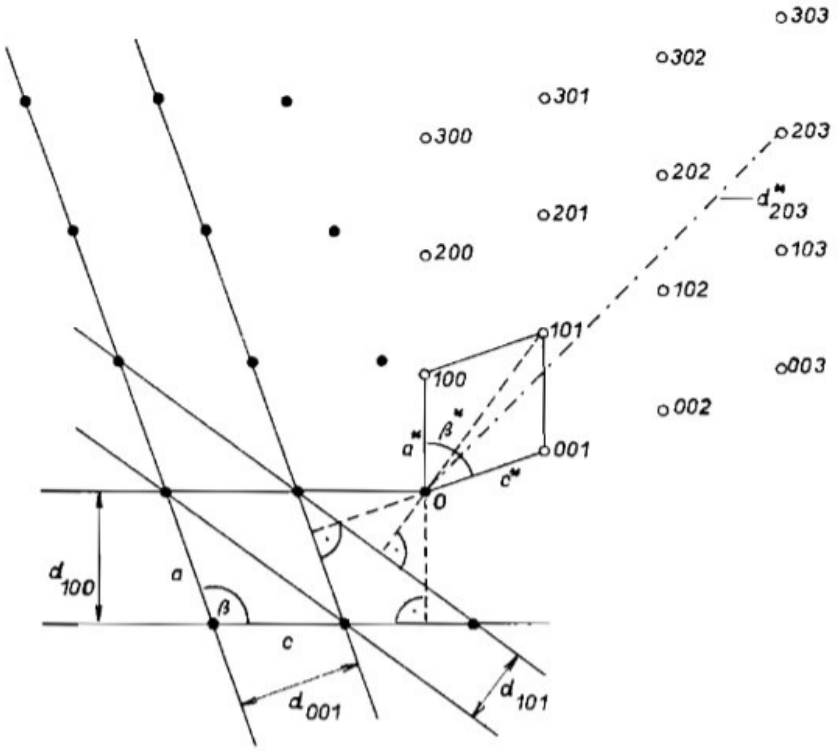

Fig. 1.1: An illustration of reciprocal lattice created from using direct crystal lattice. Image taken from [13]

1.2 Diffraction

Diffraction is an event during which a wave of any type (sound, light - photons, waves on water surface) bends from its original direction. Prerequisite for this phenomenon to happen is that waves collide with a slit of dimensions comparable to the wavelength of the initial wave. A typical depiction is a double slit experiment. Slit in case of diffraction experiments on solid states are exchanged for a crystalline material, therefore a lattice of atoms periodically ordered with slits being created between the atoms. To fulfill the prerequisite and observe a diffraction, chosen wave needs to have a wavelength comparable to the distances between atoms.

Suitable for this is electromagnetic radiation of X-ray part of a spectrum, and due to wave-particle dualism, neutrons and electrons of these wavelength can be used too. Direction and intensity of diffracted rays are dependent on the inner structure of a sample. Sample like with periodic structure like monocrystal behaves like a diffraction lattice to visible light. Intensity contributions of diffracted waves - or rather radiation, interfere with each other in specific directions given by the crystal structure, and resulting in them adding up or dimming out.

1.2.1 Diffraction on crystal

Let's assume a monochromatic (of single wavelength) wave incident onto periodically ordered atom structures, with wavelength of λ and wave-vector $\vec{\boldsymbol{k_I}}$. Next assumption is that scattering event will be elastic (in X-ray diffraction - Thompson scattering) during which diffracted wave-vector of diffracted wave $\vec{\boldsymbol{k_F}}$ remains of the same value as wave-vector of incident wave $\vec{\boldsymbol{k_I}}$, while changing the direction (therefore $\left|\vec{\boldsymbol{k_I}}\right| = \left|\vec{\boldsymbol{k_F}}\right|$). The diffraction maxima happen at points where *Laue equations* are satisfied:

$$\begin{aligned} \vec{\boldsymbol{a}} \cdot (\vec{\boldsymbol{k_F}} - \vec{\boldsymbol{k_I}}) &= 2\pi h \\ \vec{\boldsymbol{b}} \cdot (\vec{\boldsymbol{k_F}} - \vec{\boldsymbol{k_I}}) &= 2\pi k \\ \vec{\boldsymbol{c}} \cdot (\vec{\boldsymbol{k_F}} - \vec{\boldsymbol{k_I}}) &= 2\pi l \end{aligned} \tag{1.1}$$

where numbers h,k,l characterize the order of reflection and are being called *Laue indexes*. After substituting for scattering vector $\vec{\boldsymbol{S}} = \frac{\vec{\boldsymbol{k_F}} - \vec{\boldsymbol{k_I}}}{2\pi}$ resulting Laue equations are simplified:

$$\begin{aligned} \vec{\boldsymbol{a}} \cdot \vec{\boldsymbol{S}} &= h \\ \vec{\boldsymbol{b}} \cdot \vec{\boldsymbol{S}} &= k \\ \vec{\boldsymbol{c}} \cdot \vec{\boldsymbol{S}} &= l \end{aligned} \tag{1.2}$$

Lets consider the vector of reciprocal lattice $\vec{\boldsymbol{H_{hkl}}} = h\vec{\boldsymbol{a*}} + k\vec{\boldsymbol{b*}} + l\vec{\boldsymbol{c*}}$, where $\vec{\boldsymbol{a*}}, \vec{\boldsymbol{b*}}, \vec{\boldsymbol{c*}}$ are vectors of reciprocal lattice. After multiplying $\vec{\boldsymbol{H_{hkl}}}$ with vectors of direct lattice $\vec{\boldsymbol{a}}, \vec{\boldsymbol{b}}, \vec{\boldsymbol{c}}$ we obtain h, k, l to fill in equation 1.2, whereas it is possible

to conclude that during the diffraction event on a crystal the directions of scattered beams satisfy relation:

$$\vec{\boldsymbol{S}} = h\vec{\boldsymbol{a*}} + k\vec{\boldsymbol{b*}} + l\vec{\boldsymbol{c*}} = \vec{\boldsymbol{H_{hkl}}} \tag{1.3}$$

therefore vectors $\vec{\boldsymbol{H_{hkl}}}$ give us directions of beams diffracted by the crystal. Being incident on a crystal, incident beam transforms into discrete points of diffracted beams, which satisfy *Laue equations* and which can be interpreted as reflection of crystallographic planes *(hkl)*, as the following equation is fulfilled:

$$\left|\vec{\boldsymbol{H_{hkl}}}\right| = \frac{1}{d_{hkl}} = \left|\vec{\boldsymbol{S}}\right| = \frac{2sin\theta}{\lambda} \tag{1.4}$$

Rearranging the equation we get *Bragg equation*

$$\lambda = 2d_{hkl}sin\theta \tag{1.5}$$

Laue equations are fulfilled at the instant, when scattering vector is identical to some vector of reciprocal lattice. Diffractogram may be obtained by depicting reciprocal lattice by *Ewald construction*, which graphically represents the relation of scattering vector and vector of reciprocal lattice. In case of a monocrystal, this reciprocal lattice consists of points, as seen in 1.2.

Now let's consider polycrystalline material. The difference between monocrystal and polycrystal is that basically polycrystal is made of numerous monocrystals - grains. For the *Ewald construction* of polycrystalline sample we assume that there are sufficient amount of grains in sufficient amount of orientations leading to ending points of all reciprocal vectors portraying continuous spherical surfaces like in figure 1.3. These spherical surfaces are components of reciprocal lattice for polycrystalline material and easy way to imagine their formulation is by thinking of rotation of single crystal in all possible directions. cross Ewald sphere in a set of circles, therefore diffracted beams make up a set of coaxial cones which then interacts with cylindrical film around the sample. Intersection of the diffraction cones with cylindrical film are curves called diffraction lines or reflections. This film is although replaced by moving detector, recording the intesity of diffracted dependent of angle θ beams and giving us a diffractogram.

1.2.2 XRD

This work will be primarily focused on explaining the principles of neutron diffraction and in the further reading we will presume the reader is knowledgeable about X-ray diffraction, although, similarities and differences between those methods will be properly discussed in coming chapters.

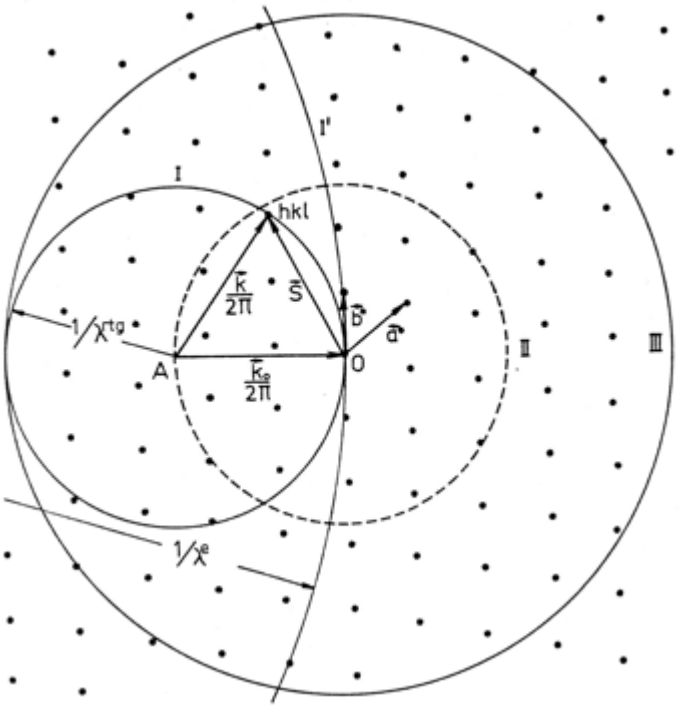

Fig. 1.2: Ewald construction in reciprocal lattice. $\vec{k_0}$ and $\vec{k}$ represent $\vec{k_I}$ and $\vec{k_F}$. Marked as I is reflection sphere for X-ray and neutron radiation. I' stands for reflection sphere of electron radiation. II represents geometrical place of centers of reflection spheres and III is a restriction sphere. Image taken from presentation of course SPL2.

1.2.3 Neutrons

Neutrons are similarly to photons and electrons also particles used to probe into solid matter and as an investigation tool to understand the way in which atoms build up different states of matter. It is this application, namely using neutron beams for examination of the structure of solid, by which this thesis is motivated. Although the theories of elastic scattering of neutron and x-ray radiation are similar (identical wavelength of both radiations comparable to distance between crystallographic planes), there is a great distinction in the mechanism of scattering those radiations by atoms. In the case of x-rays, scattering occurs on the electron cloud of the atom, while for neutron radiation it is an atomic nucleus. Exceptions are magnetic substances, where scattering happens because of the interaction of the magnetic moment of neutron and the magnetic field of electron cloud of an atom. The technique and application of neutron diffraction will be discussed as well as the possibilities it offers over a conventional X-ray method.

1.3 Crystallographic texture

Inside a polycrystalline material, the crystallographic axes of the grains may be orientated randomly with respect to each other, or they can be orientated so that there

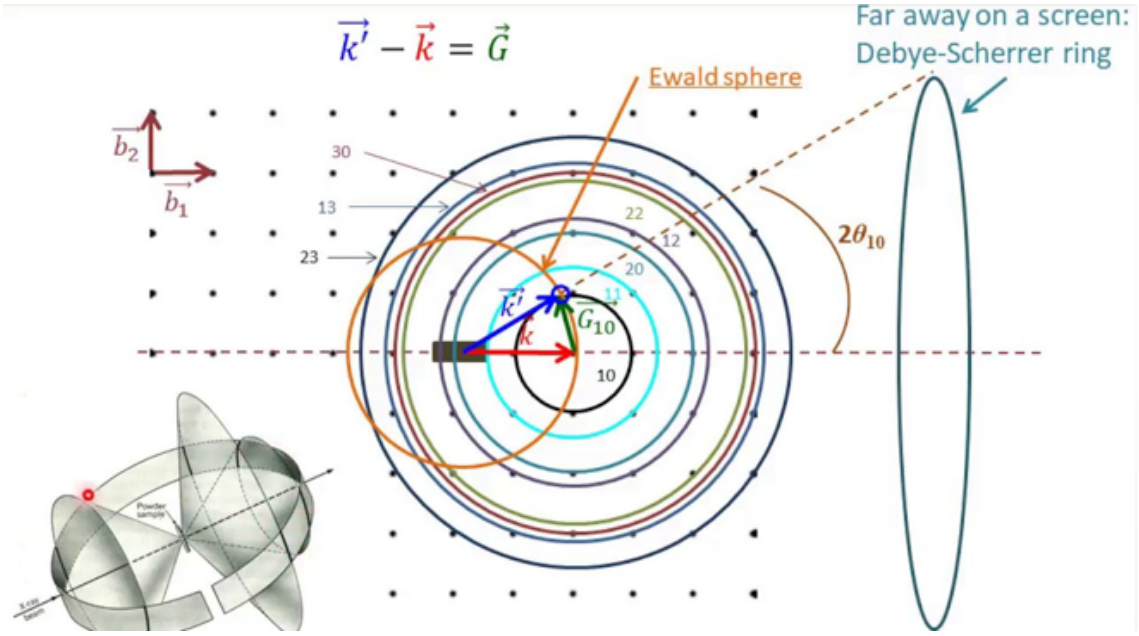

Fig. 1.3: Ewald construction in reciprocal lattice of polycrystalline material. $\vec{k}$ and $\vec{k'}$ represent $\vec{k_I}$ and $\vec{k_F}$ and $\vec{G}$ stands for scattering vector. Image taken from presentation of course SPL2.

is non-random distribution. If there is a preferred orientation, then we say there is crystallographic texture. In the past, optical methods and etching have been used to determine grain orientation, nowadays however grain orientation is determined by X-ray, neutron and electron diffraction techniques. The apparatus used for measuring textures is a four,angle diffractometer known as *Eulerian cradle*. During texture measurement, the source of radiation and the detector are oriented in such way, that a particular value of 2θ is specified. This means that a single Bragg reflection will be measured as a specified lattice plane fulfills the Bragg condition, the detector will record the reflection. The sample in the cradle is tilted and rotated systematically in order to investigate all angular orientations of the sample. For a polycrystalline material, the intensity of detected radiation will increase when there are more crystallites in a specific orientation. The intensisty for a given orientation is proportional to the volume fraction of crystallites with that orientation. Areas with high and low intensities suggest the preferred orientation, whereas constant intesity at all angles suggest random grain orientations. Different sources of radiation can lead to different depths of penetration which divides the mesurements to either surface (X-ray, electrons) or bulk (neutrons) textures.
Texture can come to existence whenever there is a preferred crystallographic orientation within a polycrystalline material. One example of precess that creates texture is solidification. A directional solidification leads to texture when columnar grains grow in preferred direction, in the heat flow direction. Crystals with a fast growth direction parallel to that of heat flow will dominate the final structure. Then there are textures that came to existence after deformation of a sample.Processes that are connected to meachanical deformation are for example rolling plates, pulling wires,

pushing through a hole. By grinding the sample into a powder the texure may as well completly disappear. Another origin of texture may be a recrystallization [7].

1.3.1 Pole figures

Pole figure is a representation of texture that is defined as a stereographic projection of spatial distribution of planes (hkl) into the projection surface parallel with some of the external frame axis[7,9]. External frame is typically defined by normal direction (ND) to the sample, the rolling direction (RD) and the transversal direction (TD) in a sheet. Pole figures therefore depicts, how are planes (hkl) distributed in an irradiated volume. If a material shows a degree of texture, the resultant pole figure will show accumulation of poles about specific directions. Only one pole figure is not sufficient for the complete determination of orientations and minimal number of pole figures is 3 for 3 different non-parallel planes.

1.3.2 Inverse pole figures

Instead of plotting crystal orientations with respect to an external frame of reference, inverse polve figures may be created showing us ND, RD and TD respectively with respect to the crystallographic axes. Typically, these are plotted on a standard stereographic triangle. Inverse pole figures depict the distribution of crystallographic planes $\{\mathrm{hkl}\}_i$ of irradiated volume in a specified direction.

1.3.3 Orientation distribution function (ODF)

More information can be gathered by creating ODF. ODFs are constructed by combining data from several pole figures. This step requires intensive use of mathematics (iteration methods WIMV [10], method of harmonic functions, etc.). ODF gives us a complete distribution of crystallites in an irradiated volume as a function $\mathbf{f(g)}$ of their orientations $\mathbf{g}$. ODFs describe the orientation of each crystal relative to three *Euler angles* (φ, ψ and θ). These angles define a difference in orientation between the crystal axes and the axes of external frame (ND,RD,TD). Considering polycrystalline sample, first step is to link every crystallite with its own coordinate system. Axes of these crystallites coordinate systems are in relation to the vectors of unit cell. Orientation of crystallites coordinate systems in relation to external frame in the irradiated volume is given by $\mathbf{g}$. Orientation $\mathbf{g}$ is parameterized by three Euler angles $(\varphi_1, \Phi, \varphi_2)$, that define three individual rotations by which external frame coordinate system is trasferred to coordinate system of crystallites.
ODF can be also interpretated as function that gives as a probability of finging crystallite with orientation g, where $g = g(\varphi, \psi, \theta)$ in an irradiated volume. Many notations are used for *Euler angles*: Bunge $(\varphi_1, \Phi, \varphi_2)$, Roe (Ψ, Θ, Φ), etc. Having computed the ODF, it is possible to reversely compute pole figures for any crystallographic plane.

Course of the orientation distribution function is observed in an areas of Euler space - in intersections of φ_1, φ_2 constant.
Orientation of crystallites is described by ideal orientations of monocrystal (IOM). By IOM it is understood such an orientation of monocrystal, in which chosen crystallographic plane (hkl) is parallel with some significant plane of external frame (like rolling plane) and appointed crystallographic direction [uvw] in this chosen plane is parallel to a significant direction of external frame [21].
During ideal orientation of crystallite its rotation related to the coordinates of external frame given by Euler angles $(\varphi_1, \Phi, \varphi_2)$, describing a point inside an Euler space. The values of ODF in the specified point can be linked to the related ideal orientation.

1.4 Diffractometer construction

The diffractometer used in the neutronographic texture experiment is localized in UJV Řež. The essential component all around the core of the nuclear reactor is the moderator - light water that slows down the high-velocity hot neutrons, produced by fission, to low energetic thermal neutrons. A nuclear reactor as a whole thus becomes the source of thermal neutrons and these can be extracted in the form of a defined beam by inserting suitable collimators leading neutrons outside of the reactor. Beam emerging from a collimator will not be monochromatic but will possess a Maxwellian energy distribution centered about its most probable wavelength. For obtaining a convenient wavelength of about 1 , a narrow band of wavelengths is separated by a crystal monochromator. A monochromatic beam of neutrons may irradiate an area of a few centimeters squared and diffract on the specimen. Detection of diffracted neutrons is done by a boron trifluoride proportional counter detector, attached to an arm that rotates around the axis of the specimen. Although principles and techniques are similar to measurements with X-rays, the scale of the apparatus is much larger [4].

Chapter 2

Neutron diffractography

2.1 Neutron

Neutron (^{1}n) is a subatomic particle and an elementary building block of all ordinary matter. Commonly, neutrons are found inside the atomic nucleus. These neutrons are "bound", as they are restrained with positively charged protons inside the nucleus by a strong nuclear force, the strongest one of the 4 fundamental forces of nature (with others being weak nuclear force, electromagnetism, and gravity) and one with a finite range of effect of about one femtometer (1×10^{-15} m), approximately the radius of a neutron. The nucleus of elements from the periodic table ranges from radii of 1-10 fm. These dimensions are far smaller than the diameter of the atom itself, as the negatively charged cloud of electrons, surrounding the nucleus, spans the layered orbitals to lengths of 0.3-3$\times10^{-10}$m from the nucleus or 0.3 to 3 Å - angstroms, unit of length often used when dealing with sizes of atoms, molecules, chemical bonds, and crystals. The radius of the whole atom is thus more than 10000 times the radius of its nucleus. The number of protons Z (the atomic number) in the nuclei determines the complete value of the charge of the nucleus as well as the chemical element from the periodic table itself. An equal amount of charge needs to be stored in a cloud of electrons orbiting the nucleus due to the long-ranged electromagnetic attraction of opposite charges, in order for an isolated atom to be neutral and in the ground state. The number and configuration of these electrons define the chemical properties of atoms, adding or subtracting electrons means the creation of anions and cations. Positively charged protons however must repel each other by electromagnetic force at close distances within the nucleus, except for protium hydrogen (^{1}p$^+$ or ^{1}H), a nucleus made of a single lone proton. Short ranged strong nuclear force overcomes the electromagnetic force and binds protons together in the nucleus while binding neutrons as well, which are required for the stability of the whole nucleus. If we change the number of neutrons inside a nucleus of an atom, we will have a different isotope of the same chemical element. This change does not result in different chemical properties but only in changed physical properties (mass of the whole atom, radioactivity ...). Some elements have a few stable isotopes that do not emit ionizing radiation, some have none.

2.1.1 Free neutron

To produce free neutrons, not "bound" in atomic nucleus, several processes can be utilized, mainly nuclear fission in the nuclear reactors. Released free neutrons are not stable but undergo a β^-decay induced by a weak nuclear force. In the β^-decay, neutron disintegrates into a proton, electron and electron antineutrino,

$$^1_0\mathrm{n} \rightarrow {}^1_1\mathrm{p}^+ + e^- + \nu^- \tag{2.1}$$

conserving the total mass and charge and by a distribution of kinetic energy between particles, the energy. Half-time of this β^-decay happening varies is according to [6] measured to be 10.61 $\pm$ 0.16 minutes from the moment neutron was liberated, depending on the method used to measure average neutron half-life. These free neutrons can be conducted through channels and collimators, shaped into beams, and used for a variety of experiments where mentioned beams come in contact with matter.

The mass of the neutron particle is slightly higher but almost equal to that of a positively charged proton. The numerical value of mass is $\mathrm{m}_n = 1.675\times10^{-27}$kg. As the name suggests, neutrons are neutral particles, meaning that the electric charge they possess is zero. Consequently, electric fields will not affect the motion of neutrons. The same cannot be said about magnetic fields. Neutrons do interact with magnetic fields, as they act as little magnets, because they possess a magnetic dipole moment μ_n = -1.913 μ_N. μ_N here signifies a nuclear magneton, a physical constant expressing magnetic moments of heavy particles, given as:

$$\mu_N = \frac{e\hbar}{2m_p} \tag{2.2}$$

where e is the elementary charge, $\hbar$ is the reduced Planck constant and m_p is the mass of a proton. Looking at the equation, by the inverse proportionality of mass, we can make a comparison with a magnetic moment of 1839 times less massive electron. Substituting m_p with a mass of an electron, which is about 1/2000 of an m_p, we reach a conclusion that the electron magnetic moment is roughly 1000 times larger. The existence of the neutron magnetic moment can be, in a very simplified manner, explained as a result of the neutron being made up of 3 elementary particles - quarks. Quarks are charged particles and their movement within the neutron as well as their own magnetic moments give birth to the total magnetic moment of the neutron. This magnetic moment has a direction given by the spin vector of the particle. When an external magnetic field is applied to the neutron, the spin vector aligns in opposite direction.

The spin of a neutron is $\frac{1}{2}$, thus making the neutron a fermion particle. Fermions are subjected to the Pauli exclusion principle, meaning that only one fermion can occupy a single quantum state at a given time. Multiple fermions together in a closed system must differ from each other in at least one property (like a spin, energy, etc.)

- they must differ in quantum numbers. This is the same reason why neutron stars do not collapse into black holes.

By virtue of the wave-particle dualism, neutrons exhibit both wave-like and particle-like properties. We are able to assign velocity (v) and kinetic energy (E) to the free neutron, as well as wavevector(k), wavelength (λ), and temperature (T). Relationships between these quantities are:

$$E = \frac{1}{2} m_n v^2 = k_B T = \frac{(\hbar k)^2}{2m_n} \tag{2.3}$$

$$k = \frac{2\pi}{\lambda} = \frac{m_n v}{\hbar} \tag{2.4}$$

$$\lambda = \frac{h}{p}, p = m_n v = \sqrt{2 m_n E} \tag{2.5}$$

where h and $\hbar$ are Planck's constant and reduced Planck's constant respectively. Boltzmann's constant is denoted k_B and p is momentum for particles of non-zero mass like neutron. The energy of a neutron is often measured in [meV], but it can also be characterized by its speed v, its wavelength λ, or its wavenumber k. For the computations, there are numerical conversion tables between the units. For example, evaluating exponential $e^{E/k_B T}$ with E expressed in meV and T in Kelvin requires one to be converted to another. Tables can be found in appendix /2/ Ampl_b1.

Another option to express the energy of the free neutron is by temperature. Term temperature is used because, when neutrons are artificially produced by a nuclear reactor, they are moderated by a medium (water or heavy water) with a certain temperature. Neutrons will collide with medium particles and lose energy, those not absorbed by the medium will eventually reach the energy level of thermal equilibrium with a medium.

For the purposes of next discussion in this thesis, we divide neutrons into groups based on their temperature 2.3. Neutron groups consist of hot, thermal, and cold neutrons. These categories also possess characteristic kinetic energy and radiation wavelength, all shown in Tab. 2.1.
Most theory will be focused on thermal neutrons in thermal equilibrium of moderator at room temperatures of 20°C and energies of 0.025 eV = 25×10^{-9} corresponding to wavelengths of about 1 Å. Precisely because of this wavelength being comparable to distances of atomic planes of solid crystalline materials, it is possible to observe diffraction of thermal neutron beam on the crystal lattice. The most probable velocity can be easily derived from Eq.(2.3) as:

$$v_0 = \sqrt{\frac{2 k_B T}{m_n}} \tag{2.6}$$

which is approximately 2200 m/s for thermal neutrons.

	Energy (meV)	Temperature (K)	Wavelength (nm)
Cold	0.1 - 10	1 - 120	0.4 - 3
Thermal	5 - 100	60 - 1000	0.1 - 0.4
Hot	100 - 500	1000 - 6000	0.04 - 0.1

Table 2.1: Table of different neutron parameters relative to each other.

2.2 Neutron interactions

Neutrons are particles that do not possess an electric charge. As a consequence, no negative electric fields from electrons in atomic clouds affect the path of free neutrons transmitting through them. The same can be said about the positive charges of protons. The interaction we observe is connected to the strong force, not the electromagnetism. Neutrons interact directly with nuclei, therefore these interactions are depicted by nuclear reaction equations.
For better understanding, we mention that the wavelength of a thermal neutron is roughly one angstrom (10^{-10}m), whereas the diameter of the nucleus is on the order of femtometers (10^{-15}m). That would mean the nucleus can be understood as a point and a solid crystalline object as a lattice of points with set distances from each other.

2.2.1 Nuclear reactions of neutrons

The scheme of a nuclear reaction comprising an excited nucleus state is as follows:

$$\mathrm{n} + {}^{A}_{Z}\mathrm{X} \rightarrow {}^{A+1}_{Z}\mathrm{X}^{*} \rightarrow \mathrm{Y} + \mathrm{p} + \mathrm{Q} \tag{2.7}$$

where n is a neutron, X represents target nuclei while X^{*} stands for target nuclei in an excited state. Y is used for an outcoming nucleus, Q for the energy produced in an exothermic reaction - $\mathrm{Q} > 0$ or consumed by an endothermic reaction - $\mathrm{Q} < 0$, and p is the product. Z is used to mark an atomic number - the number of protons in a nucleus, determining the chemical element. Nucleon number A is a count of protons and neutrons, both called nucleons, in the nucleus added up or $\mathrm{A} = \mathrm{Z} + \mathrm{N}$, where N is the number of neutrons. Nuclei of a given element (same atomic number) may have different numbers of neutrons and are then said to be different isotopes of the element. The amount of energy Q featured in equation 2.7 is computed by a formula:

$$\mathrm{Q} = 931.494 \times (n + {}^{A}\mathrm{X} - (p + {}^{A'}\mathrm{Y})). \tag{2.8}$$

Unified atomic mass unit [u] or Dalton [Da] is defined to be 1/12 of the mass of one carbon-12 atom, as carbon-12 possesses a mass of exactly 12 u. Values of variables in the equation are masses of specific elements n, X, Y, and p expressed in u. Factor 931.494 MeV comes from the conversion of the single atomic mass constant to its energy equivalent, where following is true: 1 u = 1.66×10^{-27} kg = 931.494 MeV. The energy released by the nuclear reaction manifests mainly as kinetic energy of

product particles, emission of high energy photons (γ-rays), or excitation of a nucleus (* symbol)

2.3 Nuclear processes

In the scheme of a nuclear reaction 2.7, numerous processes are introduced under which the excited nucleus progresses into a ground energetic state - decays. Product p of reaction depends on the specific type of process. The possibilities are:

(n,n)	elastic scattering
(n,n')	inelastic scattering
(n,β)	emission of β radiation
(n,γ)	emission of γ radiation
(n,p)	emission of positively charged particle
(n,α)	emission of positively charged $^4_2$He
(n,2n)	emission of neutron cascade
(n,f)	fission products + emission of neutrons

Table 2.2: List of possible products of nuclear reaction and relating processes

Elastic scattering (n,n)- neutron diffraction and inelastic scattering (n,n') are processes applied in the field of neutron scattering.

Creation of charged particles (n,β), (n,p), (n,α) as a result of nuclear reaction is a process often happening in the filling of the detectors and in the conversion sheets. Fission reaction (n,f) and cascade (n,2n) are reactions commonly describing what happens at neutron sources, conventional reactors, and spallation as well.
Neutron as a particle without an electric charge easily penetrates negatively charged atomic electron orbitals and crosses into the nucleus of an atom, therefore making the nucleus excited. Reversion of the nucleus from an excited state to the ground state can happen through the processes stated in Tab.2.2. The actual selection of which process happens is the result of the energetic level's structure of the target nucleus as well as energy of the neutron.
Except for a direct elastic scattering (n,n) or potential scattering, i.e. defection of the incident neutron by the nuclear potential, reactions do not happen directly. That means the reaction includes the formation of compound nucleus.

2.3.1 Compund nucleus

Next, we will focus on the strong interaction, natural force neutrons succumb to, in the field of nuclear forces. For the explanation and analysis of neutron interactions with nuclei, the compound nucleus model is used. It is one of the models of neutron physics, describing the structure of nuclei, often used in relation to the neutron scattering properties. The incident neutron from the source unites with the

target nucleus, producing a relatively long-lived ($>10^{-17}$s) compound nucleus. The compound nucleus has 2 stages:

1. Creation of compound nucleus - incident neutron loses its individuality in the environment of other nucleons
2. Decay of compound nucleus-nucleus decays into separate components by the transition to the ground state

1st stage Neutron penetrates inside the nucleus in a case, where it comes close enough for the strong interaction to take effect (10^{-15}m) - these nuclear forces are described by a potential well. As the incident neutron enters the nucleus between the already present nucleons, nucleus transits into an excited state, characterized by a system of energetic levels and by the energy the incident neutron possesses. Energetic levels, an energetic ladder system occurring in atomic orbitals is present in a similar way inside a nucleus.

The energy of an incident neutron is equal to the sum of its kinetic energy and the binding energy of the neutron - between 5 - 8 MeV. Graph of binding energy is shown in the appendix /3/ binding_energy. This energy is distributed between all nucleus components, therefore this energy can be as well called excitation energy. Afterward, the nucleus is ready to transition into the ground state. In this stage, a statistical probability distribution happens for some processes mentioned in Tab. 2.2 and nucleus deexcitates .

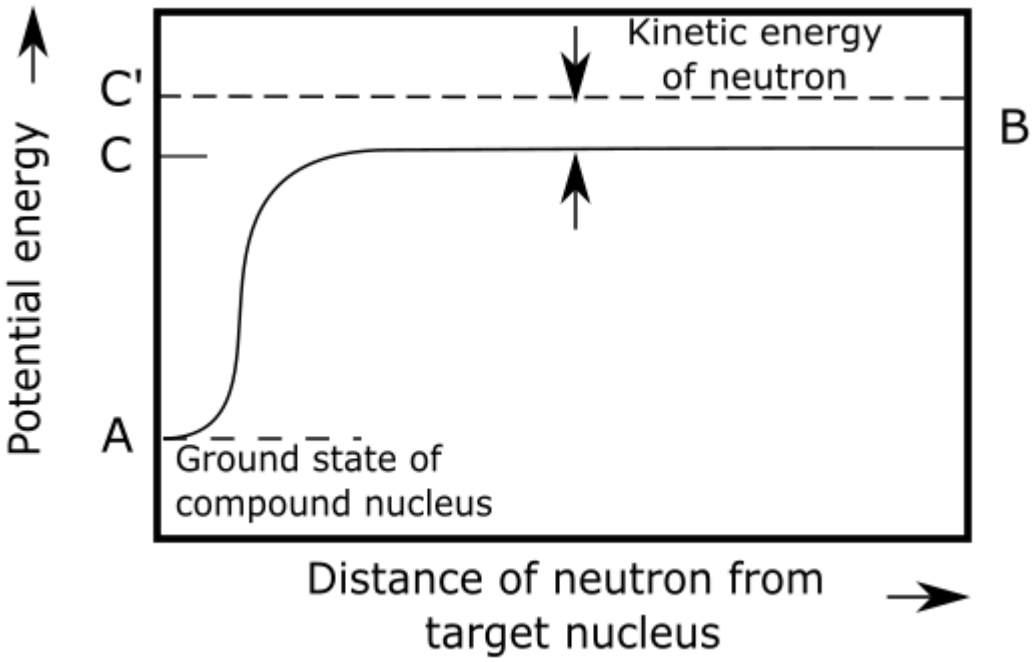

Fig. 2.1: Potential energy of system of target nucleus and neutron. Illustrated by author.

The situation can be depicted by a curve of potential energy. Figure 2.1 above shows us the energy of the target nucleus and neutron system, depending on the distance between those two. On the right side of the figure at point B, target nucleus and neutron are very distant from each other and they seem unrelated. On the other hand, at point A on the left side, it is possible to say that the target nucleus and neutron combined, therefore they produce a compound nucleus in its ground state. The difference between points A and B symbolizes a binding energy of neutron in the compound nucleus. This is the very same energy, that we would need to give to the compound nucleus in the ground state at point A, in order to free the neutron from the target nucleus and move it far from the nucleus, as in situation B.

When a neutron with zero kinetic energy comes closer to the target nucleus, the change of total energy does not occur and this energy stays equal to the energy at point B. If a nucleus absorbs this neutron, the energy of compound nucleus will be equal to point C. This nucleus is in an excited state and excitation energy is given as the length of segment AC, therefore equal to the binding energy of neutron. If the absorbed neutron had a kinetic energy, the state of the compound nucleus is described by dashed line C'. Excitation energy, in this case, is the length of AC' segment. The conclusion is: If a compound nucleus is created by neutron capture, the excitation energy (the excess energy above the ground state of a compound nucleus) is equal to the binding energy and kinetic energy of the incident neutron.

It is important to mention, that previous speculation is valid only in case when target nucleus has infinite mass. In general case, if neutron and nucleus collide, and a neutron capture happens, the resulting compound nucleus gains kinetic energy, because of impulse conservation. Because of this, only a part of neutron energy turns into the internal excitation energy of compound nucleus. However, if a target nucleus is sufficiently heavy, practically all of the energy is converted to excitation energy. This statement will be considered true for the purposes of the next discussions.

Conditions for the compound nucleus to manifest and processes of following emissions of products of the reaction are determined mostly by the density and width of energetic levels of the target nucleus and energy of the incidental neutron. An example of such energy levels is shown in figure 2.3. The probability of formation of a compound nucleus is dependent on and rises in cases, when the sum of incident neutron kinetic energy and binding energy is close to a resonance level. Compound nucleus formation is a resonance reaction, meaning that it can be only formed if the sum of kinetic and binding energies of incident neutron corresponds to an excited state of the compound nucleus.

It is assumed, that the increase in speed of a specific nuclear reaction happens when the energy of incident neutron is such that the created excited state of compound nucleus is very close to one of its quantum energy levels. This phenomenon is named resonance absorption. Resonance absorption is illustrated in figure 2.2, where straight lines on the right side schematically illustrate quantum energetic states of the compound nucleus. The dashed line marked E_0 signifies a sum of energy of the target nucleus and binding energy of neutron with nonzero kinetic energy. Relative to the figure 2.1 we see, that E_0 stands for the same amount of energy as in point

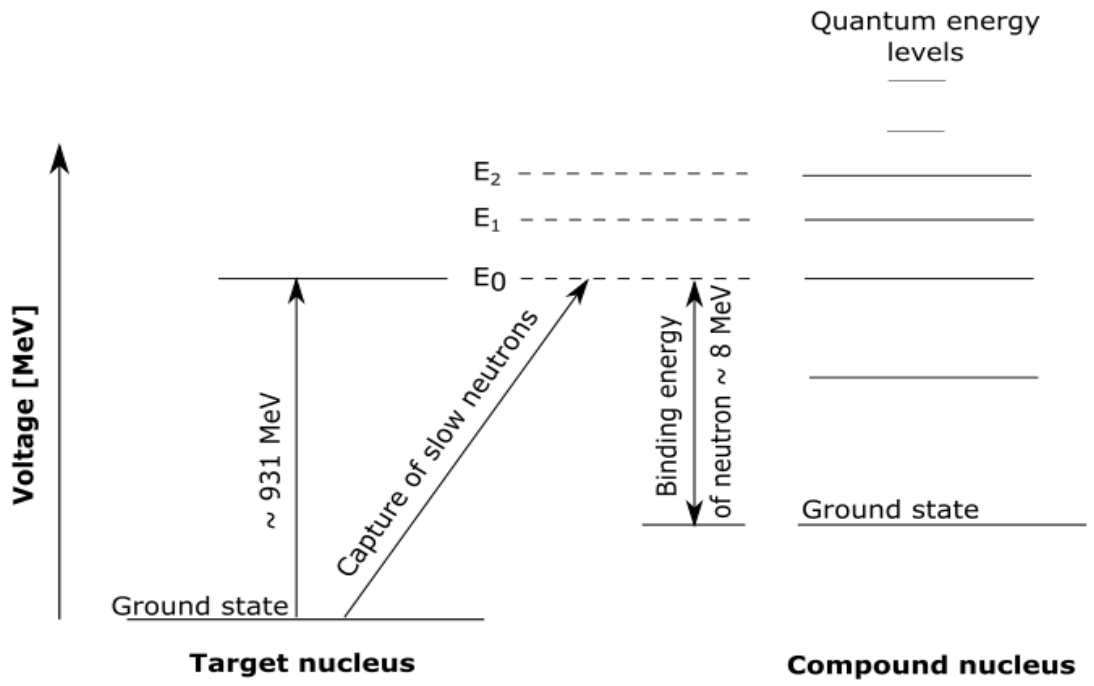

Fig. 2.2: Potential energy of system of target nucleus and neutron.Illustrated by author.

C. This energy is by a value of binding energy of neutron in a selected compound nucleus higher than the energy of the ground state.

2nd stage For sufficiently high excitation energies, the compound nucleus can decay by emitting charged particles or a cascade of neutrons [(n,α) (n,p),(n,2n)]

If the energy of an incident neutron is not sufficient for the emission of a particle, the excited nucleus turns into the ground state by emitting a γ radiation (n,γ).

Also, when a nucleus emits a particle, it is possible that some energy may remain, making it still excited. In this case, a nucleus emits a γ radiation as well. A neutron with kinetic energy smaller than that of the incident neutron can also be emitted, remaining nucleus stays in an excited state which subsequently decays by γ radiation (inelastic scattering).

In the heaviest nuclei, fission can occur.

Another possibility is for the neutron with the same energy as the originally captured neutron to be emitted (n,n). Due to the capture, this process is called compound elastic scattering or alternatively resonance scattering. This process is an elastic collision.

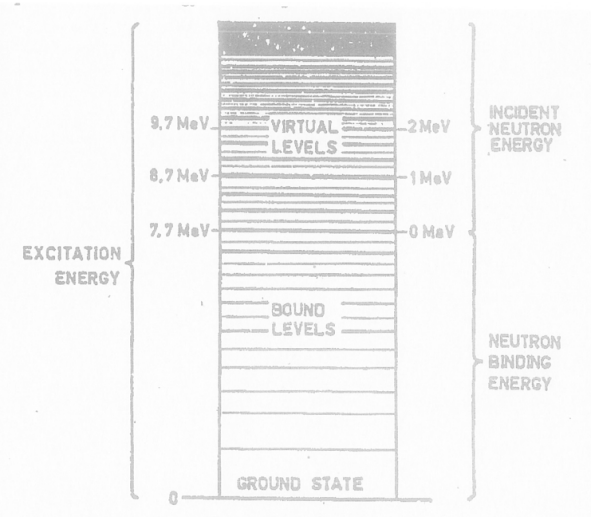

Fig. 2.3: Potential energy of system of target nucleus and neutron. Image provided by consultant.

2.4 Neutron cross-section

For the quantitative characterization of nuclear reactions, the microscopic neutron cross section denoted as σ is used [1].
In the simplest terms, this neutron cross-section is the area, an effective target area around a single nucleus which numerically expresses the probability of nuclear reaction (any from section 2.3), induced by an incident neutrons of a certain energy. The greater the value of the microscopic cross-section, the higher the probability of reaction. As it describes a surface, the cross-section is measured in units of the area - m^2. This unit is however too large in comparison to areas around atomic nuclei, so instead, the unit **barn** is used as standard. One barn [b] is equal to 10^{-28}m. The most important thing that determines the actual value of the microscopic cross-section is the energy of incident neutrons. Cross-section as a function of energy depicts different values depending on how many MeV of kinetic energy incident neutrons possess or instead we can perceive it as dependence on the temperature (cold, thermal, hot) of neutrons.

Each reaction has its own corresponding cross-section but the simplest distinction is made between:

1. scattering processes (n,n) and (n,n'), where neutron makes and elastic or inelastic collision with a nucleus - σ_s
2. absorption or capture processes, in which neutron disappears inside a nucleus and causes various secondary radiations to appear - σ_a

An approach to classifying all individual isotopes (nuclides) is by the determination of particular neutron cross-sections and by the ways how it reacts with the incident neutron. Some isotopes are more inclined to absorb neutrons and then either decay or stay excited, those isotopes will naturally possess a capture cross-section σ_a.

Boron-10 ^{10}B is such an isotope, with neutron cross-section of its (n,α) reaction for thermal neutrons (0.025 eV) of about 3840 barns. Gadolinium isotopes ^{155}Gd and ^{157}Gd are very good absorbers of neutrons as well, with their capture cross-section of reaction (n,γ) for thermal neutrons being 61 000 barns and 254 000 barns respectively.

Another set of isotopes is ones that undergo fission. Isotopes like that possess fission cross-section. An example for those fissile isotopes would be uranium-235 with fission cross-section σ_f for thermal neutrons of about 585 barns. For fast neutrons, this value drops to the order of barns.
All other isotopes will simply scatter the incident neutrons, therefore possessing a scattering cross-section σ_s. Isotopes like uranium-238 ^{238}U possess all three mentioned cross-sections as seen in figure 2.4:

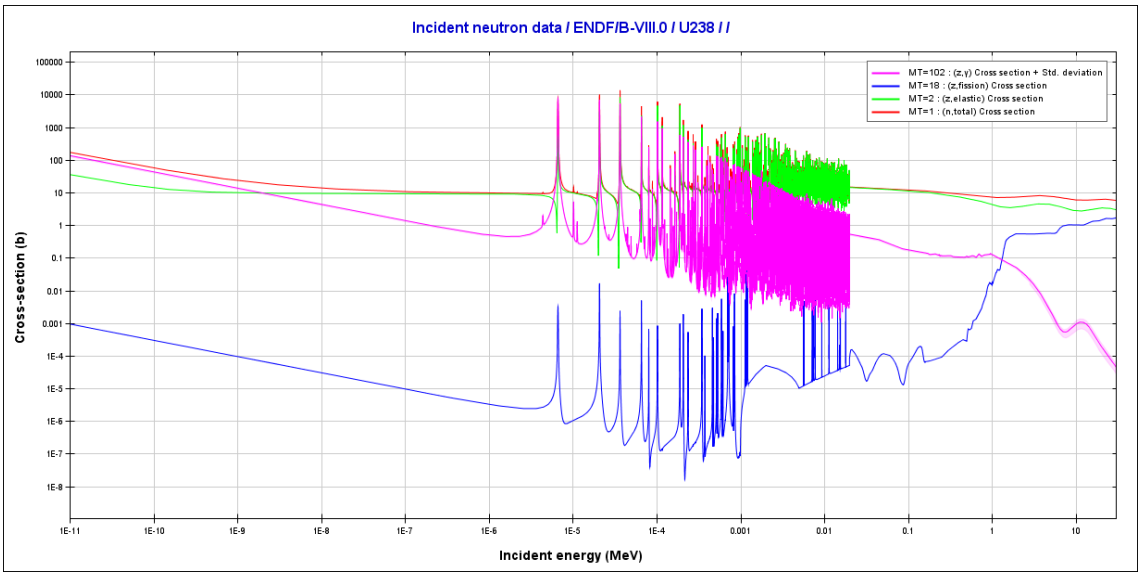

Fig. 2.4: Plot depicting some cross-sections of isotope uranium-238. Source:JANIS; database: ENDF/B-VIII.

2.4.1 Total cross-section

All of the neutron-induced nuclear processes described in 2.3 are denoted by a characteristic cross-section. Elastic scattering is described by elastic scattering cross-section σ_e, inelastic scattering by σ_i, radiative capture by the capture cross-section σ_γ, fission by σ_f, and so on. All of these possible nuclear cross-sections measured together give us a numerical value of what is called total cross-section σ_t. The total cross-section is the sum of all possible cross-sections:

$$\sigma_t = \sigma_e + \sigma_i + \sigma_\gamma + \sigma_\alpha + ... \tag{2.9}$$

and it measures the probability that any type of interaction will happen as neutrons strike the target. Absorption cross-section σ_a is also made of partial cross-sections of all absorption reactions:

$$\sigma_a = \sigma_f + \sigma_p + \sigma_\gamma + \sigma_\alpha + ... \tag{2.10}$$

where σ_p and σ_α are cross-sections for the (n.p) and (n,α) reactions. By convention, fission is too treated as an absorption process [2]. Scattering cross-section σ_s is also a sum of particular cross-sections:

$$\sigma_s = \sigma_e + \sigma_i \tag{2.11}$$

and final total cross-section can be seen as a simple sum of scattering and absorption cross-sections:

$$\sigma_t = \sigma_s + \sigma_a \tag{2.12}$$

2.4.2 Neutron cross-section data

Plots of individual cross-sections dependent on incident neutron energy for mostly any reaction with any isotope can be found in data libraries, such as the Evaluated Nuclear Data File database (current version ENDF/B-VIII). Taking data from this database, by using the application JANIS (Java-based Nuclear Data Information Software), real cross-section data were prepared to discuss:

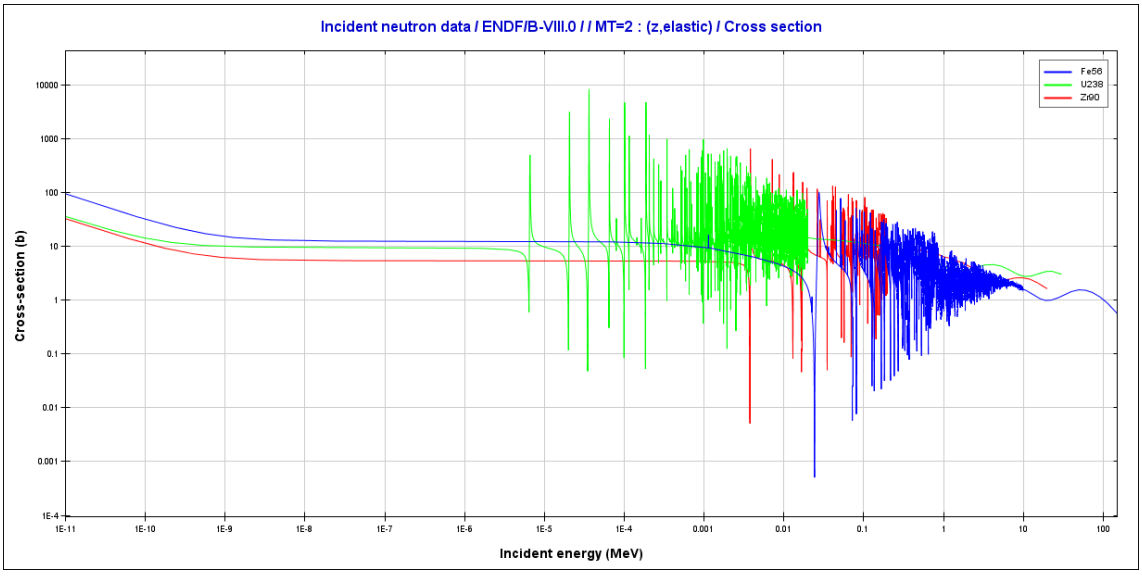

Fig. 2.5: Plot depicting elastic scattering cross-sections of intermediate and heavy isotopes. Source: JANIS; database: ENDF/B-VIII.

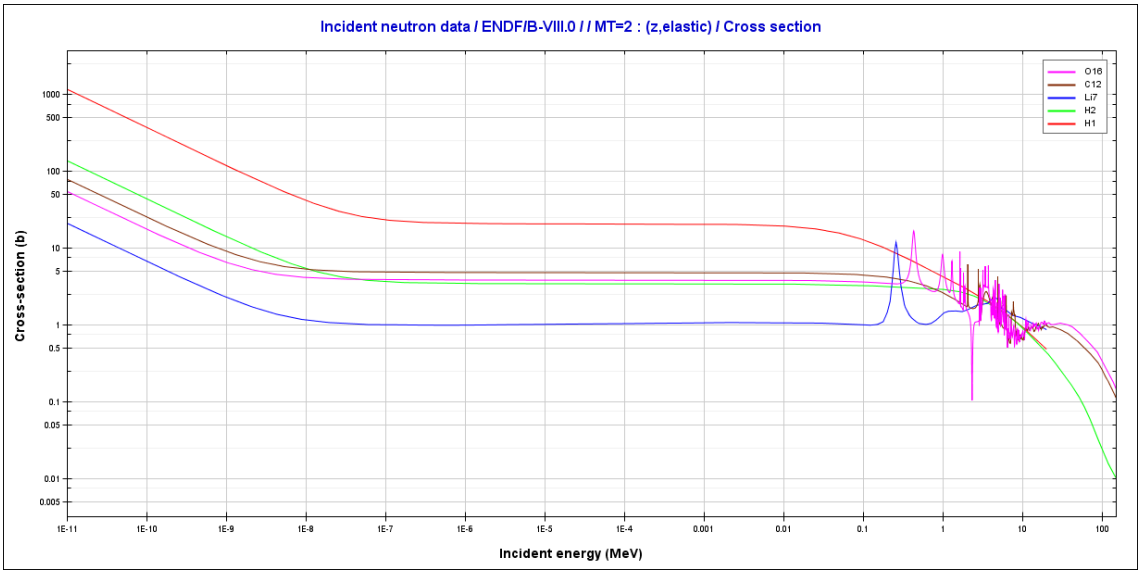

Fig. 2.6: Plot depicting elastic scattering cross-sections of light isotopes Source: JANIS; database: ENDF/B-VIII.

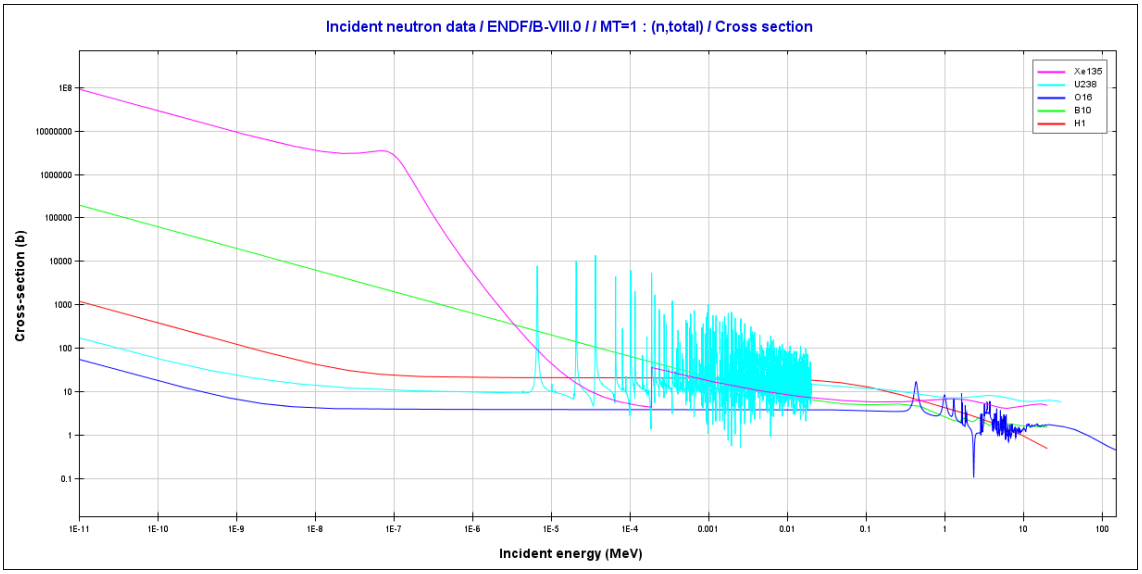

Fig. 2.7: Plot depicting total cross-sections of a few important isotopes Source: JANIS; database: ENDF/B-VIII.

From figures 2.6 and 2.5 we may observe that light elements act practically independent of neutron energy up to the energies of 1 MeV, orders of magnitude higher than thermal neutrons. This means the scattering cross-section behaves like a constant for thermal neutrons. It is similar for intermediate and heavy isotopes as well, but the resonation maximas show at lower neutron energies.
These maximas called resonances are a striking feature of interactions that evolves by the compound nucleus formation. Resonances occur at certain incident neutron energies in what is called the resonance region of cross-section plots. The way these

energies are distributed is connected with energy levels discussed in a chapter 2.3.1. It was shown that nuclei possess excited states, which are the result of the inner configuration of nucleons. What we observe in plots are probabilities of incident neutron and target nucleus combining spiking up whenever is incident neutron energy precisely right amount to create compound nucleus in one of its excited states. Resonances show up in the cross-section because it is necessary to form the compound nucleus before interaction can proceed [2]. In 1st stage of the Compound Nucleus, it was shown that it takes energy - the neutron binding energy, to pull neutron away from the nucleus. This energy also reappears, whenever a neutron enters the nucleus. Consequently, when the neutron collides with a nucleus, the compound nucleus is formed in an excited state possessing energy equal to the sum of incident neutron kinetic energy and the binding energy of the neutron in the compound nucleus.

Elastic scattering We observe from figures 2.5 and 2.6 that σ_e as a function of the energy can be divided into four distinct regions. Cold neutrons and very low-energy region, where the value of cross-section rises as the energy of incident neutrons lowers. One simple explanation is that neutrons are passing through the nucleus effective area for a longer time. Next, the low energy regions that can be approximated by constant, because scattering in this region does not happen by the formation of a compound nucleus, but simply because of forces exerted by the target nucleus on the passing neutron. This is a region of potential scattering, and the cross-section value is given by a simple equation for the surface of the ball:

$$\sigma_e(\text{potential scattering}) = 4\pi b^2 \tag{2.13}$$

where b acting as a radius is a scattering amplitude specific for every isotope. Beyond this region of elastic scattering follows a region of resonances caused by compound nucleus formation. Full equation of elastic scattering cross-section in the neighbourhood of resonance maximas is given by Breit-Wigner dispersion equation :

$$\sigma_e(\text{potential scattering}) = 4\pi\left|\xi^2 + \frac{const.}{(E - E_r) + \frac{1}{2}(\Gamma_n^{(r)} - \Gamma_a^{(r)})}\right|^2 \tag{2.14}$$

where ξ is the number describing potential scattering, it is always positive and it is equal to the geometric radius R of the target nucleus. E is the energy of incident neutron, E_r signifies the energy needed for the formation of resonance level in the compound nucleus, lastly, $\Gamma_n^{(r)}$ and $\Gamma_a^{(r)}$ are widths of resonances for repeated emission of neutrons with original energy and for absorption. The whole second term in equation Eq.(2.13) is a resonance term, its value rises as the value E_r comes close to E (the resonance energy level becomes close to the thermal energy of neutrons). Expression *(E - E_r)* may acquire both negative and positive values, $\Gamma_n^{(r)}$ and $\Gamma_a^{(r)}$ are always positive. Under the specific conditions, the resonance term can be negative and high enough, to numerically outweigh potential term ξ and give as final scattering amplitude b negative (this happens for isotopes like ^{1}H,^{7}Li, etc.) [3].

At even higher energies these resonances start to lose individuality and squeeze together, forming a smooth continuum region where σ_e becomes a slowly varying function of energy. In this region of high energies, the continuum region can be also looked at as an outcome of the insufficient resolving power of neuron spectrometers which are used for cross-section measurements.[1]

2.4.3 Nuclear scattering length b, scattering amplitude

Denoted as b, the scattering length of a nucleus is in fact equal to the amplitude of the scattered neutron beam at a unit distance from the scattering nucleus, for an incident beam of unit amplitude [4]. What this shows us is how easily the nucleus scatters the neutron. The value of scattering length is determined by a quantum mechanical scattering process. A wave representing an incident neutron ($\lambda \approx 1 \times 10^{-10}$m) interacts with a point nucleus (diameter of few fm - d $\approx n \times 10^{-15}$m, n < 100). With ratios like these, the Schrodinger equation is solved in a Born approximation. In this approximation, the scattering amplitude acts as a constant, isotropic in the interval of thermal neutron energies. The order of scattering amplitude is on the same order as the real geometric radius of a nucleus, but not equal. The importance of scattering length is hidden in fact, that it is a measure of how effectively a nucleus scatters incident neutrons. By considering quantum mechanical solutions to the process of nuclear scattering, it can be concluded that scattering cross-section and scattering length are in relation. Actual values of scattering amplitudes and sets of cross-sections for individual elements are determined experimentally and recorded for example inside tables like the appendix: /1/: Ampl_Rozpt_b.doc.

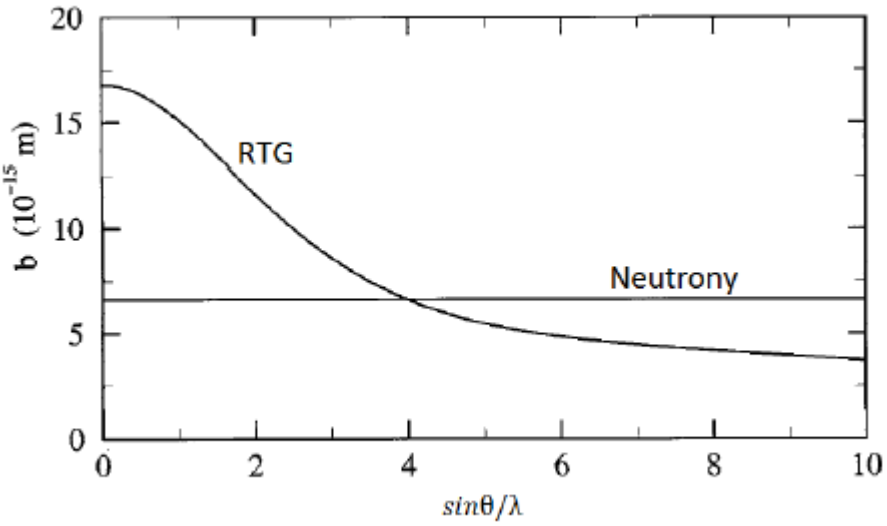

Fig. 2.8: Dependance of scattering amplitude b on diffraction angle θ. Source: [5], modified.

Comparison of dependence of neutron scattering length b and X-ray form-factor

on $\frac{sin\theta}{\lambda}$ is schematically depicted in figure 2.8. The scattering amplitude of thermal neutrons does seemingly not depend on the angle of diffraction θ, therefore scattering is anisotropic. For the X-ray, the radiation weakens and the amplitude of scattered waves falls for high angles θ.

The dependence of scattering amplitude b on the atomic number A is shown on figure 2.9. Equivalent X-ray quantity of linearly dependent form-factor is shown in the figure as well, so the great distinction between X-ray and neutrons may be seen. Relation for neutron scattering length plays important role in structure analysis during determining positions of light elements (H, Li, B, etc.) and during distinguishing positions of elements with proton numbers close to each other. Few nuclei possess a negative value of scattering amplitude b, namely H, ^{7}Li, ^{48}Ti, ^{51}V, Mn and ^{62}Ni. Case of manganase, for example, can be correlated with known scattering resonances at incident neutron energies of 300 eV and 2400 eV.

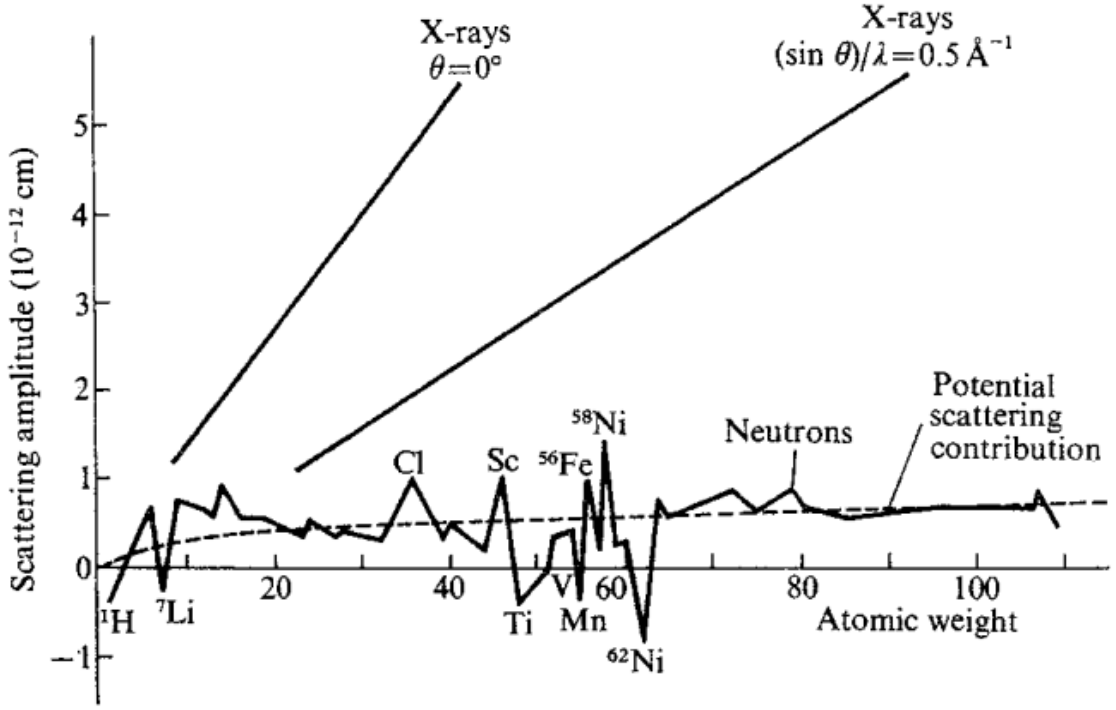

Fig. 2.9: Coherent scattering lengths of x-rays and neutrons (b)
as a function of atomic number. The discussed dependence of X-rays on $\frac{sin\theta}{\lambda}$ is taken into consideration. Source: [4]

2.4.4 Macroscopic cross-section; transmission experiment

A common way of inducing nuclear reactions is the bombardment of some sort of target nucleus with incident neutrons. However, we already know that nucleus is a very tiny object and a vast majority of an atom is an empty space. So in this kind of experiment, we need to make calculations with a slab of material. The vast

majority of incident neutrons bombarding a thin slab however penetrate through without any kind of interaction. Now is it possible to calculate how many of incident neutrons will actually interact with the target nucleus and lead to some kind of nuclear reaction and also calculate how many particles will pass through ? For that, it is necessary to know a nuclear neutron cross-section of a reaction we observe. If it is known what isotopes is a slab of material composed of, using 2.13 it is possible to calculate cross-section with knowledge of scattering amplitude b.

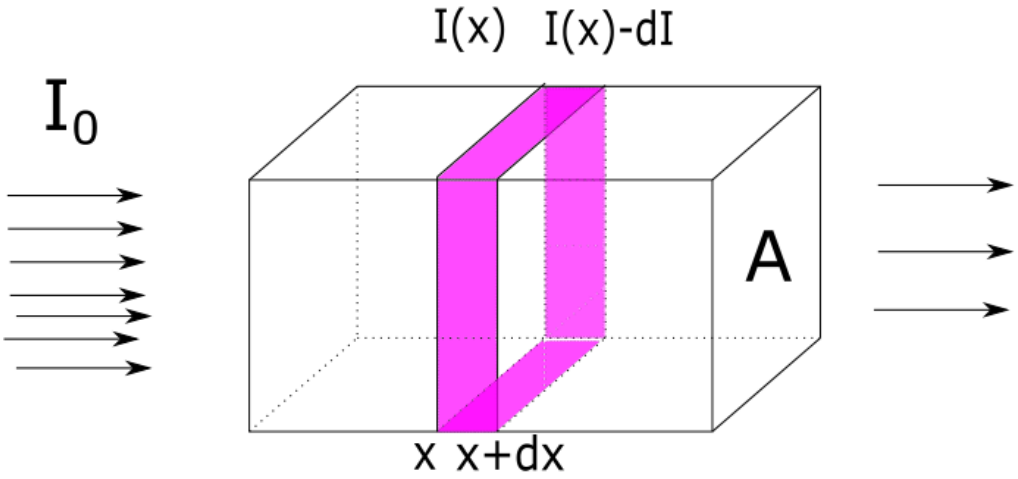

Fig. 2.10: Simple sketch of transmission experiment

Let's consider experiment in diagram 2.10. On the left side, there are incident neutrons with a defined number I_0, incident onto some kind of material. A rectangular slab of material, containing a target nucleus. Let x direction be the direction of the neutron flow. Next, let's suppose the area of slab facing the incident neutron beam is **A**. Suppose we take a very small slice of a slab material having a thickness of **dx** and area of **A** (in diagram depicted by fuchsia color). Now, we will try to answer how many nuclear interactions happen in this particular slice. Important quantity to define is **I(x)** which signifies the number of incident neutrons at the distance x. Now after penetrating distance **dx**, this quantity is going to decrease, so it evolves into **I(x) - dI** at the distance **x** + **dx**. Quantity **dI** must consequently be the total amount of interactions in a slice (if there is only one interaction per particle) or according to another definition: a decrease in the number of incident particles. Another quantity we need to compute how many interactions will take place in a slice is, how many target nuclei exist within the slice. **N** [cm^{-3}] notes a number of atoms per unit volume in the used material. For calculating the number of atoms **N** in one cm^{-3} of a substance, the simplified equation for a monoatomic substance (like graphite) is:

$$N = \frac{\rho}{M_A} N_A \tag{2.15}$$

where ρ stands for a density of a substance, M_A stands for atomic mass and N_A is Avogadro's number. A number of target nuclei within the slice is simply equal to **NAdx**. Now to add to this number a characteristic proportionality constant, that will correspond to each isotope - elastic nuclear cross-section σ_e - an area of interaction corresponding to one nucleus. If **NAdx** is multiplied by this quantity, an actual area of a slice that is available for interaction will be given as **NAdx**σ_e, also called an effective plane of cross-sections.

Now it is possible to make a statement, that an effective plane of cross-section **NAdx**σ_e divided by an area of irradiated slice **A** is going to be equal to the ratio of the number of interacting neutrons in a slice **dI** to the original value of neutrons before the sliced bar of slab **I(x)**. Putting that into the equation gives:

$$\frac{dI}{I} = \frac{NA\sigma_e dx}{A} = N\sigma_e dx \tag{2.16}$$

N$\sigma_e$dx therefore signifies amount of interaction in a small slice upon the total number of incident neutrons. We can integrate this expression over certain amount of distance:

$$\int_{I_0}^{I} \frac{dI}{I} = -\int_{x=0}^{x} N\sigma dx \tag{2.17}$$

It should be obvious here that since the number of particles is decreasing, we need to introduce a minus sign, therefore change in the number of particles is negative. Following modifications:

$$[lnn]_{I_0}^{I} = -N\sigma x \tag{2.18}$$

$$ln\frac{I}{I_0} = -N\sigma x \tag{2.19}$$

lead to deriving a final relationship for **I(x)** that tells us how the number of incident particles changes as it penetrates into some kind of material:

$$I(x) = I_0 e^{-N\sigma x} \tag{2.20}$$

We observe an exponential decrease in the number of particles that survive penetrating through the material. Such a simple expression can help us calculate how many of the incident neutrons will pass through the material of defined thickness or how many of those will lead to the interaction. An example of how function **I(x)** behaves is shown in figure 2.11.

Frequent use is made of the quantity

$$\Sigma = \sigma N \tag{2.21}$$

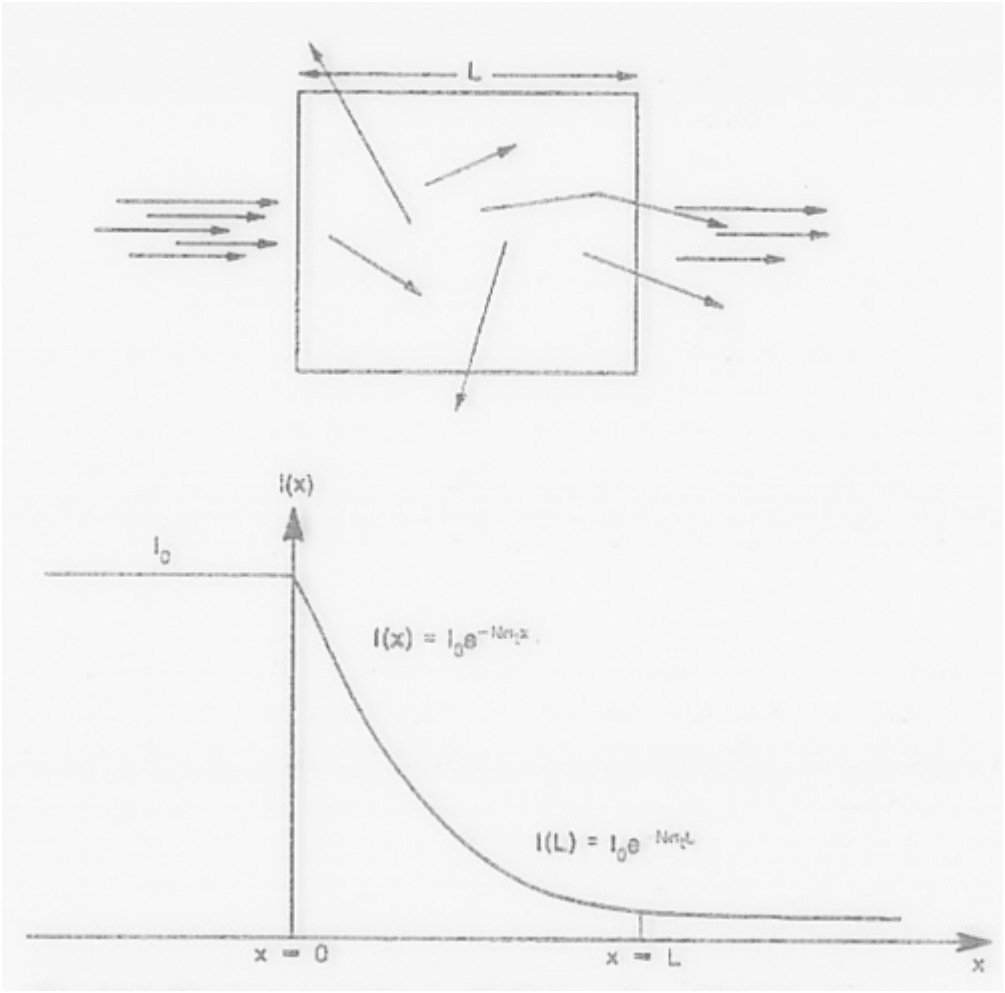

Fig. 2.11: The intensity of a parallel beam of uncollided neutrons decreases exponentially as it passes through a thick layer of matter

called macroscopic cross-section. It specifies the cross-section per cm^3. It can also be considered as the probability that the neutron is scattered or absorbed in a path 1 cm long.

2.5 Neutron diffraction

2.5.1 An elastic scattering of neutrons

If we assume the wave-like properties of neutron, elastic scattering would be a reflection of a neutron wave from the nucleus and absorbtion of neutrons would be weakening of the wave inside of nucleus. Elastic scattering can happen by 2 possible mechanisms. In the first one, neutron is scattered in the potential field of nuclear forces of target nucleus. This scattering is also called potential scattering.
Next possibility arises when neutron penetrates inside the nucleus and creates compound nucleus in excited state. This compound nucleus can transit to the ground

state by emission of a neutron in a way, which preserves laws of conservation of kinetic energy and momentum. As a result of discrete energy levels, compound nucleus cannot form at any energentic level, only at the ones, where sum of target nucleus energy and neutron energy is quantum permissible. Dependence of probability of this mechanism on the energy of neutrons shows a number of resonance peaks, when neutron kinetic energy fulfills the creation condition of one of discrete energy levels of compound nucleus. This is called resonance scattering.

2.6 Neutron instruments

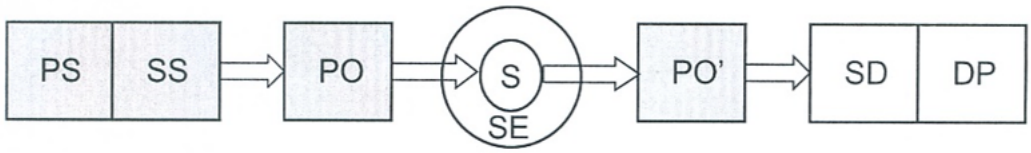

PS	Primary source	**D**	Sample
SS	Spectrum shifter	**SD**	Signal detector
PO	Phase space operator	**DP**	Data processing system
SE	Sample environment (pressure, temperature, magnetic field)		

Fig. 2.12: Basic neutron diffraction experiment scheme

A general neutron diffraction experiment is practically expressed in a graphic way in figure 2.12. Neutron sources radiate neutrons into the space isotropically, therefore they need to be moderated and focused into beams. We characterize those beams by a vector $\vec{k_I}$. Reflected (diffracted) vector $\vec{k_F}$ is determined by detector parameters (entry direction of the beam and the energy/wavelength of neutrons). Characteristics of $\vec{k_F}$ are determined by operations in phase space, namely defining direction of the beam and the intensity value. Objective of the general diffraction experiment is to determine quantities of **momentum transfer** $\hbar\vec{Q}$ and **energy transfer** $\hbar\vec{\omega}$ between the specimen and neutron. This can be achieved by many different combinations of incident and scattered neutron momenta $\vec{k_I}$ and $\vec{k_F}$. For $\hbar\vec{Q}$ and $\hbar\vec{\omega}$ to be determined with sufficient precision, the momenta $\vec{k_I}$ and $\vec{k_F}$ have to be appropriately defined and of the right magnitude. This is the main task underlying the design of neutron scattering facilities. The restriction in development of diffraction facilities being impossibility of instrument which covers most of the **Q-**ω with sufficient resolution and sufficient flexibility. The instruments developed have verying requirements with respect to spectral properties and time structure, therefore the source and the instrument designers have to interact ever more closely in conceiving new systems. There does not exist one optimal concept, but the different concepts can be optimised to suit their purpose. Current neutron scattering instruments are designed in either **continuous** mode or **time of flight** mode. Experimental data

used in next chapters were obtained by the former instrument, therefore thesis focuses on this particular method.

2.7 Sources

Neutron sources can be characterized by 3 properties: 1 - **Intensity** which is proportional to neutron yield ; 2 - **Spectrum (E,λ)**; 3 - **principle of neutron generation**, 3rd one being further subdivided by the type of nuclear reaction (product of fission or by an incident particle), while approach to heat moderation plays role of an important factor.

Alternative neutron production methods

Different methods to generate neutron flux exist, although only few of them are sufficient for use in diffraction experiments. Processes creating free neutrons such as firing **D** (deuterium $[1p^+, 1n]$) into **T** (tricium $[1p^+, 1n]$) confined in solid target or *Deuteron stripping* (stripping neutrons out of incident **D**) - firing **D** at energies of tens of MeV to generate a fusion-like neutron spectrum from the liquid ^7Li in the Li(d,n) or similarly firing at solid target of ^9Be, are unfortunately inefficient to use in diffraction experiments owing to the low neutron yield and technical difficulties occurring due to high temperatures generated by them. In similar position is the method of using a nuclear photoeffect, an attempt to induce neutron flux by using electrons in MeV/GeV range to produce e^-*bremsstrahlung* photons (emitted by decelerated electrons) which later interact with target in resonance region - ejection of neutrons by evaporation and in pulses. In the future, there is possibility of applying nuclear fusion as an efficient stable source of neutrons for diffraction experiments. As for now, this option is unavailable and currently, there are only 2 sustainable sources of neutrons used for diffraction, as highlighted in tab 2.2.

Nuclear reactors

Sources may be described mathematically by value of neutron flux $\Phi(t)$ as a function of time. In case of constant sources, the given equation is:

$$\Phi(t) = const.. \tag{2.22}$$

Most of nuclear reactors operated for neutron scattering are built as constant sources. Currently, there is only one pulse TRIGA type nuclear reactor adapted to neutron scattering experiments - IBR-2 situated at Dubna, Moscow region, Russia and relation for a pulse source is simply:

$$\Phi(t) = f(t) \tag{2.23}$$

Another way to characterize nuclear reactor is by the output, typically, research reactors being either medium or high output category . The fission process (although

Nuclear process	Example	Neutron yield	Heat release (MeV/n)
D-T in solid target	400 keV deuterons on Tin Ti	4*10-5 n/d	10 000
Deuteron stripping	40 MeV deuterons on liquid Li	7*10? n/d	3 500
Nuclear photo effect from e‘-bremsstrahlung	100 MeV e on 238	5*10? n/e	2000
9Be (d,n) 10Be	15 MeV d on Be	1 n/d	1000
8Be (p,n;p.pn)	11 MeV p on Be	5*10? n/p	2000
Nuclear fission	fission of 235U by thermal neutrons	1n/fission	180
Nuclear evaporation (spallation)	800 MeV p+ on 238U on Pb	27 n/p 17 n/p	55 30

Tab.2.2: List of the neutron sources with their respective examples, neutron yields and heat release of the specific nuclear reaction

only the general one with ^{235}U) is displayed on figure 2.12 and written in language of nuclear reaction in 2.24. Inside the reactor, the core generates neutrons of various energies (moderate - fast) at orders of keV/MeV. For both, fission sustainability and extraction of neutrons for experiments, these neutrons have to be cooled down, therefore diffused in the active zone of reactor and moderated (C,H_2O,D_2O) to lower energies of $\sim$ 100 meV. Further functionality of moderator is being an adjustment medium of neutron spectrum, and it will be discussed.

$$^{235}_{92}\mathrm{U} + ^{1}_{0}\mathrm{n}_{\mathrm{thermal}} \rightarrow {}^{236}_{92}\mathrm{U}^{*}_{\mathrm{excited}} \rightarrow 2 \text{ fission products} + \sim 2.5 \cdot {}^{1}_{0}\mathrm{n}^{\mathrm{prompt}}{}_{\mathrm{slow-fast}} + \sim 180\mathrm{MeV} \tag{2.24}$$

Energy of approximately 180 MeV is distributed between fission products while 2 or 3 neutrons, that were created during the fission of nucleus possess kinetic energy of 1-2 MeV, making them according to Tab. 2.1 fast. Load of heat produced in the fission process is unfortunately accompanied by technical difficulties with transporting the heat out of active zone, thus causing main restriction on amount of a neutron flux. The work needed to provide for the refrigeration of litre of a moderator is $\sim$ 10 kW litre of moderator. As for the pulse reactors, pulses are the results of either sudden movements of the reflector (IBR-2) or part of fuel (IBR-30 - older version of IBR-2). Fuel of mentioned pulse reactor is causing heavy distinction between normal nuclear reactor and pulsed one, that is the place of moderation being **the fuel itself**, due to confinement of fission material in matrix of moderator. Detailed workings of pulse reactors is a topic for further work. To sum up nuclear reactors, energy deposited into creating 1 neutron is roughly 180 MeV. Fission reaction is self-sustaining as long as there is enough slowed-thermal neutrons upholding the chain reaction. Development of NR has reached the limits due to heat removal problems from the fuel and because of advancement in spallation neutron sources, deployment of new reactors has been slowed down.
As for the method of leading neutrons as out of active zone of reactor, process is realized through horizontal channels. Formation of neutron beams starts at horizon-

tal channel that is either *radially* or *tangentially* oriented with respect to the active zone.

Spectral distribution of neutrons

Neutrons can be labeled into types by difference in the *temperature*, since they are being moderated by a medium, which possess certain temperature. Resulting neutrons belong to ranges of energies shown in tab. 2.1, which represent free neutron's kinetic energy, usually given in electron volts. If neutrons are in thermal equilibrium with atoms composing the moderador, it's valid to express de Broglie's wavelength of neutrons λ as:

$$\lambda = \frac{h}{mv} = \frac{h}{\sqrt{3mkT}}, \text{ because } \frac{1}{2}mv^2 = \frac{3}{2}kT \tag{2.25}$$

Beam of thermal neutrons acquires a Maxwellian distribution of velocities **??** known for thermal motion (rise in temperature = rise in kinetic energy), therefore the **spectrum (E,λ)** is continuous.

Thermal distribution of prompt neutrons in reactor active zone is show on figure 2.15a. Distribution for lower and higher moderator temperatures are shown in 2.15b and 2.15c respectively. Using de Broglie's relations, wavelength of neutrons can be obtained in place of energy and the distribution of the wavelength of neutrons is displayed at 2.14.

2.7.1 LVR-15 and channel HK-2

Used for this study was a reactor LVR-15 belonging to *Nuclear Recearch Institute* (NRI) and stationed at the *Center for Fundamental and Applied Neutron Research* (CFANR) in Řež, Czech Republic. LVR-15 is medium output ($\Phi(t) \sim 10^{13}$ n/cm^2·s) light water swimming pool type reactor with force cooling. The maximum reactor power is 10 MW thermal power. Reactor core is situated in the reactor vessel (outer diameter: 2.3 m; total height of the vessel: 6.23 m) made of steel while the internal parts are made of aluminium alloy. Simplified scheme can be seen at figure Within reactor, process described previously takes place. NRI operates the reactor LVR-15 on a commercial basis. Installed within the active zone of LVR-15 are openings of 9 horizontal channels ($\ominus$) and 2 vertical channels, directing moderated electrons to experimental instruments equipped on respective channels. Maximum thermal neutron flux out of horizontal channel (100×60 mm) of reactor LVR-15 is $\Phi_{\ominus}(t) \sim 10^8$ n/cm^2·s, which is the actual neutron flux in channel HK-2 and available for instrument: **Two-Axis Powder Diffrectometer KSN-2** stationed on this channel. Further parts of mentioned diffractometer used in this study will be discussed in coming sections.

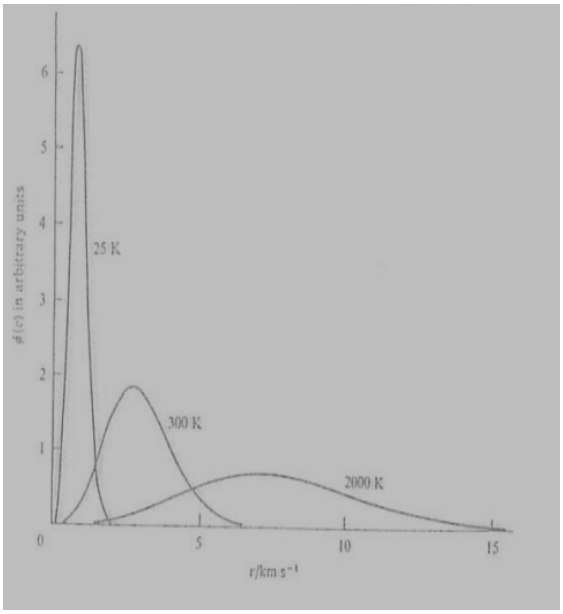

Fig. 2.13: Maxwellian flux distribution $\Phi_v \propto exp(-mv^2/2k_BT)$ for $T_1 = 25°K$, $T_2 = 300°K$, $T_3 = 2000°K$, with curves normalized to have the same area.Figures provided by consultant.

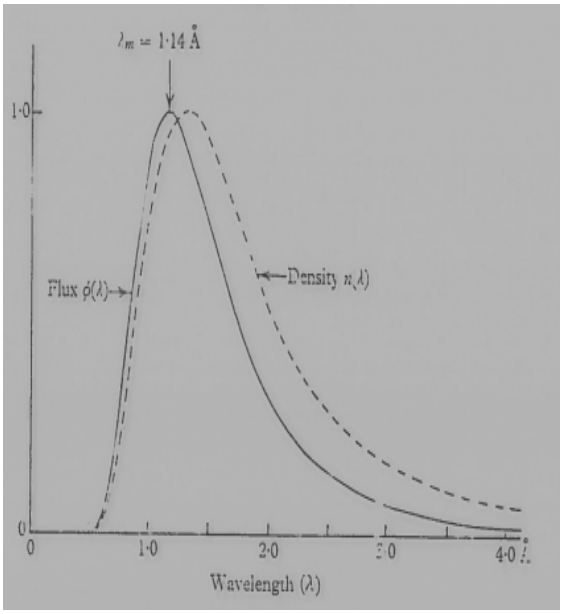

Fig. 2.14: Wavelength distribution of neutrons
in equilibrium with moderator at temperature
T = 20℃. Full curve is neutron flux emarging from collimator, broken curve is neutron density in reactor core. Curves are shifted towards shorter wavelength for higher values of the moderator temperature.Figures provided by consultant.

2.8 Collimator

A collimator is an optics system used for creation of a narrow parallel bundle of beams (collimated beam from now on) out of divergent beams. For visible light this can be realized by lenses, but due to short wavelength of both thermal neutrons and X-rays no lenses can be used for focusation. Collimator is therefore simplest optics tool for this cause. Applied to neutrons, collimators are devices used for escorting particles flying in parallel to a specific direction. In case where collimators are not used, neutrons from many directions would pass through the sample and the detector may record instances like divergent neutron flying downwards through the top of the sample. Image created in this way would be blurry and unavailing. Collimators thus improve the resolution, although due to filtering of divergent neutrons, the intensity of collimated beam drops. In neutron scattering, standard type of collimator used is the type Soller 2.17. It consists of thin alternating parallel aligned steel plate layers of neutron absorbing material and neutron permeable material. Divergence of a Soller slits alone can be computed simply as

$$\alpha = \frac{w}{L} \tag{2.26}$$

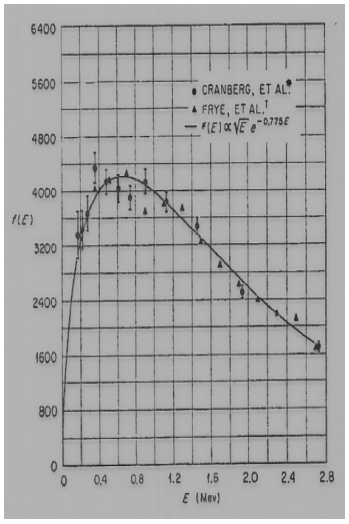

(a) The energy distribution of prompt fission neutrons (E in Mev) in active zone approximated by a function: $f(E) \approx exp(-1.036E)sinh(\sqrt{2.29E})$

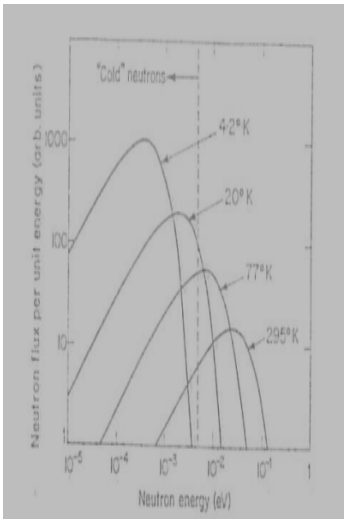

(b) Maxwellian distribution for low moderator temperatures

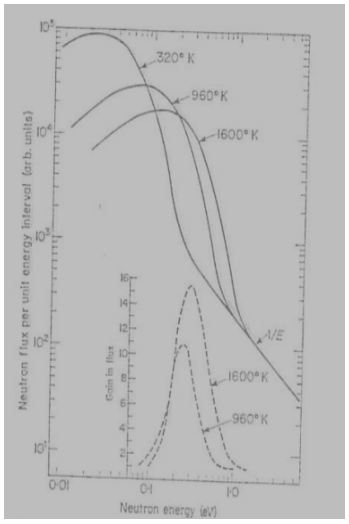

(c) Maxwellian distribution for high moderator temperatures. Insert shows rato of 960°K and 1600°K

Fig. 2.15: Energy distributions of neutrons. Figures provided by consultant.

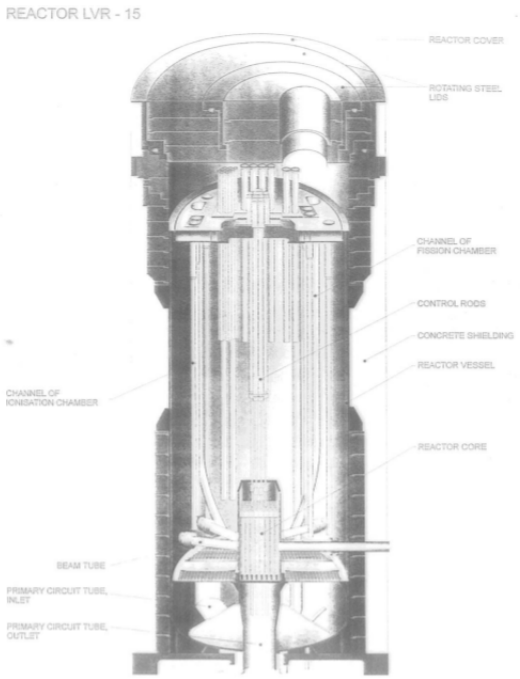

Fig. 2.16: Reactor LVR-15.Figures provided by consultant.

where w is distance between slits (mm) and L is lenghth of slits (m). Aim is for the minimal α value. It is also necessary to take into account factors as: shapes of borders of the slits and their thickness (μm). Significant role in effectivity plays

doping of steel plates in gadolinium Gd atoms or coating them by Gd, because of the accompanying nuclear reaction

$$^{157}_{64}\mathrm{Gd} + ^{1}_{0}\mathrm{n}_{\mathrm{thermal}} \rightarrow ^{158}_{64}\mathrm{Gd}^{*}_{excited} \rightarrow ^{158}_{64}\mathrm{Gd} + \gamma + 7.9\mathrm{MeV} \tag{2.27}$$

where in the place of γ rays and energy are products in fraction of reactions the auger electrons. To detect the conversion of these relatively low energy particles is difficult, as reaction is hard to discriminate from background events in the detector. This is precisely desired effect, as it is needed to detect neutrons. Collimators are also used as a front part of detectors to filter incoming neutrons from the sample. The summary: collimators are used for divergence adjustment. Neutron collimation can be beneficial in two areas: first, The probe neutron beam itself can be shaped by the collimators to reduce beam divergence leading o image blurring on the detector; and second, the collimators may be placed between the studied sample and the detector for scatter rejection for filtering divergent scattered neutrons.

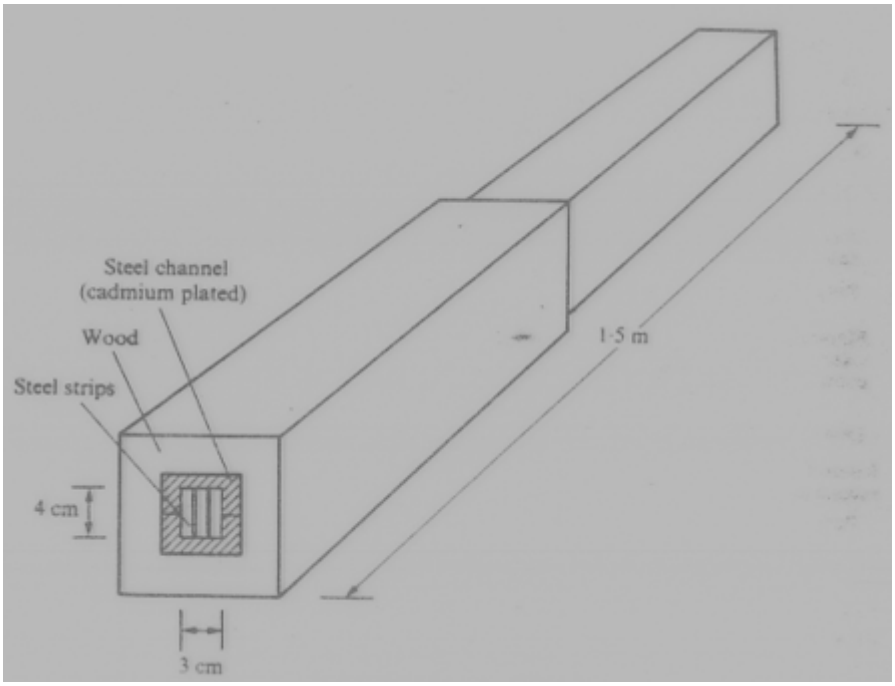

Fig. 2.17: Sketch of collimator.Figures provided by consultant.

Collimators at KSN-2 diffractometer

2.9 Monochromator

A monochromator is necessary device for constant neutron sources diffractometers placed between the collimator leading from the source and collimator leading to the sample. The beam which emerges from the source collimator is polychromatic, meaning it possess a Maxwellian distribution of energy. a narrow band of wavelengths of about 1 Åcan be separated from it by using crystal monochromator. The width

of this wavelength band, which must be contrasted with the characteristic lines used in X-ray work, will largely be determined by collimation. In practice a compromise has to be made between reducing the bandwidth by narrowing the angle of the collimator and, at the same time, maintaining an adequate number of neutrons in the incident beam[4]. In the earliest experimental work metallic halide ionic crystals, marticularly LiF, NaCl and CaF_2, which were available as large, almost perfect, single-crystal ingots. However, the intesity reflected by such crystals is low precisely because of their perfection, their mosaic spread is only one or two minutes of an arc. The reflected intensity can be increased by mechanically straining the crystal, for instance, by bending or squashing it or by roughening its surface. It was shown later that crystals of metals such as lead and copper gave intensities which were greater by a factor of two or three times, and these are now generally used.The monochromator may be used in either the ' reflection' or ' transmission' position. The latter requires a much smaller crystal for intercepting a given width of beam, but the former is more often used in order to take advantage of the 'foreshortening' technique for X-rays.

2.10 Detector

Detecting neutrons comes with an obstacle, which is the absence of electric charge in the particle. This means a detection cannot be done by standard or rather, direct observation of an electric pulse. While neutrons does not succumb to coulombic interaction, they do interact by nuclear forces and these result in nuclear reactions. Products of certain nuclear reactions (2.27) tend to possess electric charge and kinetic energy. These products are used as secondary detection particles. For example, if neutron is captured by ^{3}He, the decay of excited nucleus results in creation of 573 keV proton and 191 keV tritium, which inevitably ionize other particles in their path. All types of detectors work on principle of these secondary particles detection and process of creating them is called conversion.

Nuclides helium-3, lithium-6, boron-10, uranium-235 are great candidates to be used in conversion process, therefore as converters (their respective reations with thermal neutrons: 2.29; 2.30; 2.28; 2.24). This is due to the fact, that their neutron absorption nuclear cross-section is exceptionally high as seen in tab. ,thus materials infused with those isotopes are most likely to react with thermal neutrons. While value of cross-section is heavily dependent on the energy of neutrons, previous statement is true for thermal, intermediate and fast neutrons in comparison to most of other elements of periodic table and isotopes. Detectors are thereby compounds of: 1. Converters creating charged particles ; 2. Detectors of charged particles.

Requirements for materials used as converters and detectors are: large cross-section of used reaction, high released energy (for detection of low energy neutrons) or high conversion of kinetic energy (for fast neutrons), the possibility of discriminating between photons and neutrons (to not misinterpret γ-rays as neutrons) and lastly , being as cheap as possible. With all of these taken into account, developed types of detectors are following:

2.10.1 Ionization chambers

Ionization chamber is in general an electrical device used to detect various types of ionizing radiation. Purpose of this detector in both X-ray and neutron diffraction is mostly monitoring the intensity of beams. Chamber is composed of a cylindrical vessel filled with neutral gas and 2 concentric electrodes connected to source of constant voltage. Gas after being exposed to radiation separates to ions and electrons, or ion-pairs. With applied voltage to electrodes, such that electric field prevents recombination of these ion pairs, these charged particles are drifted towards electrodes. Positive ions drift towards cathode, negatively charged electrons towards the wire anode. This voltage does not surpass a level in which gas amplification happens (secondary ionization and avalanches). The number of ion-pairs collected by the electrodes is equal to the number of ion-pairs produced by the incident radiation and also depends on the type and energy of the incident radiation particles/rays.

A thin layer of material sensitive to neutrons, therefore the converter, covers both of the concentric electrodes. Such a device is often called fission chamber and as converters are used ^{10}B and highly enriched ^{235}U. As seen in equation 2.24 a thermal neutron causes an atom of uranium-235 to fission, resulting in 2 fission fragments produced possessing high kinetic energy. These fragments then cause ionization of argon (Ar) or dinitrogen (N_2) gas inside cylindrical vessel. ^{235}U coating offers an advantage against ^{10}B that the fission fragments have much higher energies than the alpha particle produced in boron reaction 2.28. In case of fission chambers the carbon dioxide (CO_2) is mixed to the gas filling for the purpose of rising electron mobility.

$$^{10}\mathrm{B} + {}^{1}\mathrm{n}_{\mathrm{thermal}} \rightarrow {}^{11}\mathrm{B}^{*} \rightarrow {}^{4}\mathrm{He} + {}^{7}\mathrm{Li}^{*} + 2.79\ \mathrm{MeV} \tag{2.28}$$

$$^{3}\mathrm{He} + {}^{1}\mathrm{n}_{\mathrm{thermal}} \rightarrow {}^{1}\mathrm{H} + {}^{3}\mathrm{H} + 0.77\ \mathrm{MeV} \tag{2.29}$$

2.10.2 Gas proportional neutron counters

Gas proportional counters are regularly used for the neutron detection at the constant flux 2.22 sources facilities. Their build shown on figure 2.18 is similar to fission chambers to the extent of concentric electrodes lined with ^{10}B and cylindrical vessel. The gas filling used is based on converter nuclear reactions 2.28 and 2.29, therefore He gas enriched by isotope ^{3}He and BF_3 gas enriched by isotope ^{10}B. Then an interaction happens between neutron and a sensitive material nucleus, particles are released into gas and ionize the gas all along their trajectory.

All around the wire anode there is a strong electric field due to the very small diameter of the wire. In contrast with ionization chamber, the voltage applied to electrodes in proportional counters is higher (1 - 3 kV), in fact high enough for the released electrons that migrate towards wire anode to be accelerated. Due to

sufficiently intense electric field to provide electrons with necessary energy, they themselves become ionizing and an avalanche phenomenon occurs, which enables multiplication of the electrons produced. The signals obtained are pulses. Registered pulses are from the ionization by the heavy particles ^{1}H, ^{3}H, ^{4}He or ^{7}Li, and also γ-ray photons. These γ-rays are present mainly due to photoelectric effect which produces low amplitude pulses, lower than those produced by neutrons. Charge corresponding to thermal neutrons is proportional to the energy released by nuclear reaction and it leads to pulses of amplitude high around 5 V. This difference of amplitudes is advantageously used to eliminate the gamma contribution and to conserve only the signal useful for neutrons. For this, an amplitude discrimination technique is put into effect which takes into account only those pulses higher than a specific threshold.

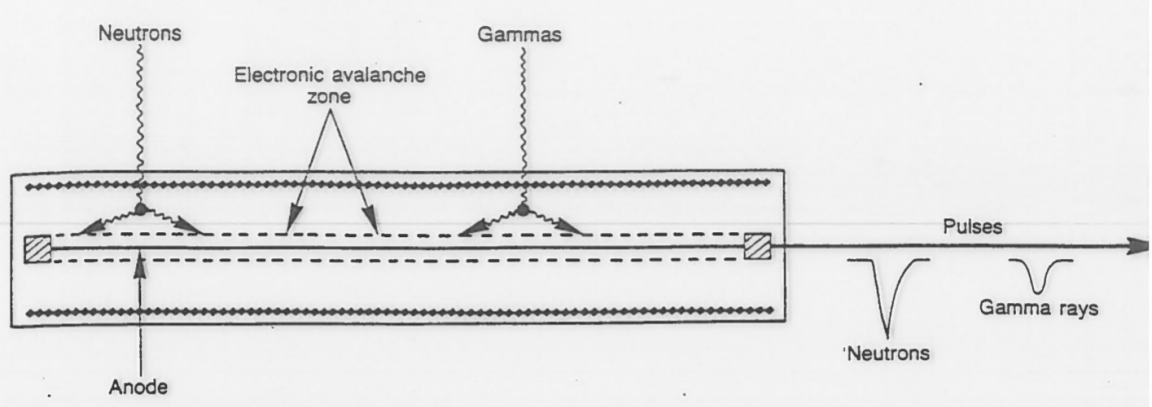

Fig. 2.18: Proportional multiplication counter diagram.Figures provided by consultant.

Proportional detector filled by BF_3

Elemental boron is fundamentally not gaseous, so boron based neutron detectors use colourless corrosive highly toxic gas BF_3 - boron trifluoride enriched by ^{10}B. Sensitivity of the boron lined fission chamber is lower than that of proportional counter as the ion-pairs are produced inside the layer. Charged fission products, alpha particle ^{4}He and lithium nucleus ^{7}Li both have sufficient energy to cause secondary ionization in the gas. They lose some of their energy while passing through the boron layer to the chamber's gas domain, while some of them are unable to enter. The number of ionizations is thus lower, than in case where neutron reacts directly with gas, as fission products here possess maximum energy and produce more ionizations. BF_3 can also be used to detect intermediate and fast neutrons (up to 10 MeV). In this case however, the detector must be surrounded by a moderating material such as polyethylene to slow down the neutrons before capture. Cadmium filters are used to porvide a uniform energy response.

Proportional detector filled by ^{3}He

In nuclear reaction 2.29 we see the formed products are tritium nucleus ^{3}H and a proton ^{1}H. It is these charged particles which produce secondary ionization. Helium proportional counters can be used for neutron spectroscopy purposes as well as detection of intermediate and fast neutrons, while using moderator. Sensitivity of ^{3}He based detector to γ-rays is low, which makes it ideal for measurements, although the ^{3}He isotope is scarce in supply as it's production relies on decay of tritium ^{3}H. Tritium itself is rare costly byproduct of nuclear reactor operations.

The neutron absorption cross-sections of both nuclear reactions are sufficient for these detectors, set to pressure of several atmospheres and widths of a few cm, to reach efficiency nearing 100%. A real detector filling is a result of various compromises: cross sections of reactions are inversely proportional to the speed of neutron, pressure of filling is set to be such that epithermal and fast neutrons have low efficiency and create a background, energetic resolution of charged particles (not neutrons) sufficient enought to discriminate γ-rays.

2.10.3 Scintillation neutron detector

In case of scintillation detector, neutrons are absorbed by a plastics or glass material of scintillator (a material which produces light when an ionizing radiation passes through it) enriched by converter isotope ^{6}Li and ZnS. Scintillation detectors are mostly used during time-of-flight (TOF) method located at pulse neutron sources. The charged particles produced by the reaction:

$$^6\mathrm{Li} + {}^1\mathrm{n}_{\mathrm{thermal}} \rightarrow {}^3\mathrm{He} + {}^4\mathrm{He} + 4.79\ \mathrm{MeV} \tag{2.30}$$

form an excitations of electrons in the scinitillator. The annihilation of these excitations results in emission of visible light spectra photons. These photons advance through the waveguides to the photomultipliers. A large amplification is needed because primary signal is low. where they are detected. Silver activated zinc sulfide ZnS(Ag) is characterized by release of great light output after the collision with α-particles ^{4}He or charged atoms of light elements.
Taking into account the high sensitivity to γ radiation, scintillation detectors are not suitable for the registration of low counts. Introduction of γ radiation filter based on shape discrimination of pulses greatly improved characteristics of scintillation detectors. As the scintillator thickness (few mm) is far lower compared to gas detectors the accurity of measurment of neutron flight period increases.

2.10.4 Position sensitive detectors

All detectors mentioned above were types of a point detectors, which transformed the problem of neutron detection using the nuclear reactions to problem in detection

specific charged particles. Aim of position sensitive detectors is to obtain one or two dimensional position information from these charged particles. In the same manner as with X-rays, the most straightforward way to manufacture position sensitive detector is to create an array of discrete point detectors. Gas proportional counters are widely available and come in variety of lengths and diameters for this purpose. In a similar manner, making an array of scintillaitors is too a viable option for acquiring a position sensitivity. Scinitllators however do not require the bulky containers holding a high pressure gas, therefore can be made much smaller and placed closer together than gas detectors.
Other type of position sensitive detectors consist of nonmosaic detector with high resistance anode and a "banana detector" - variation of gas detector composed of multiple parallel electrodes set in single vessel, shaped like part of torus.

2.11 Neutron applications

Neutrons are used in many different ways to study materials. Basic research in materials science is about clucidating structures of solids and liquids and dynamical information of atoms and molecules in them. Same can be applied to biology research. In industry, neutrons are used for production of isotopes or transmutation doping of silicon. In radiography, neutrons are used for materials analysis via activation. This is very useful in quality surveillance in metallurgy, electronics, paper and textiles, geophysical exploration and safeguards.

2.11.1 Applied neutron diffractometry

Let us mention some examples of the various investigations to which neutron diffraction measurements have contributed significant information. The main applications fall into five classes.

1. Structural investigations of solids which aim to discover the positions of light atoms, particularly hydrogen atoms. another principal applications are measurement of residual stress in components, microstructure of metals and porous media and texture of materials. Important to mention are possible *In situ* studies of chemical reactions and catalysis.

2. problems that are often found within alloy systems, which require distintion to be made between atoms of neighbouring atomic number, and which therefore have very similar scattering amplitudes for X-rays - one of X-ray drawbacks that makes neutron diffraction complementary method

3. investigations of magnetic materials, in which advantage is taken of the additional scattering of neutrons which occurs for atoms possessing magnetic moments - another convenience over X-ray methods

4. vibrations, including magnetic vibrations, which can be studied by inelastic scattering

5. studies of departures from perfect order - liquids, gases and defects

Chapter 3

Experimental part

3.1 Bivalve shells

Biologically controlled mineralization is a topic connecting scientists of many different specializations and methodologies. For that reason mollusc shell microstructures pose a ideal candidate for study. Being build of complex aragonite (or/and calcite) layer intergrowths, it is of interest in science fields like geology, as shells are the most commonly preserved fossil parts. They are used to gain infromation about phylogenetic evolution and as a marker for determining age of geological formations. In medicine, nacre was significant even 2000 years ago as dental implants. Zoologists, molecular biologists and paleontologist all have shared interest od ascertaining the inner workings of biomineralisation inside molluscs shells, therefore making the formation of molluscan shells one of most studied cases of biologically controlled mineralization.
As a model for shell formation and shell growth let's consider model proposed by A.Checa in 2000 [16] depicted on 3.1. At the time of active shell secretion the periostracal groove (A, inset 1) secretes outer periostracum, periostracum being the organic layer of the shell. Inner periostracum is secreted by the inward-facing epithelium of the mantle (A,inset 2). The periostracum reflects at the shell edge and calcification starts with the prismatic layer - the outer layer of the shell made by calcite/aragonite prisms, at the shell edge (A,inset 3) and at the certain distance from the margin initiates the growth of nacreous layer - inner hard layer of the shell. In B, mantle enters inactive period, both the shell and inner periostracum cease to be secreted, while outer periostracum continues to merge forward from periostracal groove (B, inset 1). Folds start to emerge as inner periostracal conveyor belt remains motionless (B, insets 2a and 2b). These folds are later incorporated into shell surface as growth lines. Part C shows a shell during prolonged period of mantle inactivity whereas mantle retracts and outer periostracum detaches from the periostracal groove and ceases to be secreted. Free expelled periostracum forms a marginal bundle. Part D describes the process of restarting secretion. First only the inner periostracum is secreted and in time if followed by outer periostracum (D, inset 1). As mantle fold extends, the isolated inner periostracum is transferred to the outward-facing face if the fold and to the internal surface of the shell. E. Once the

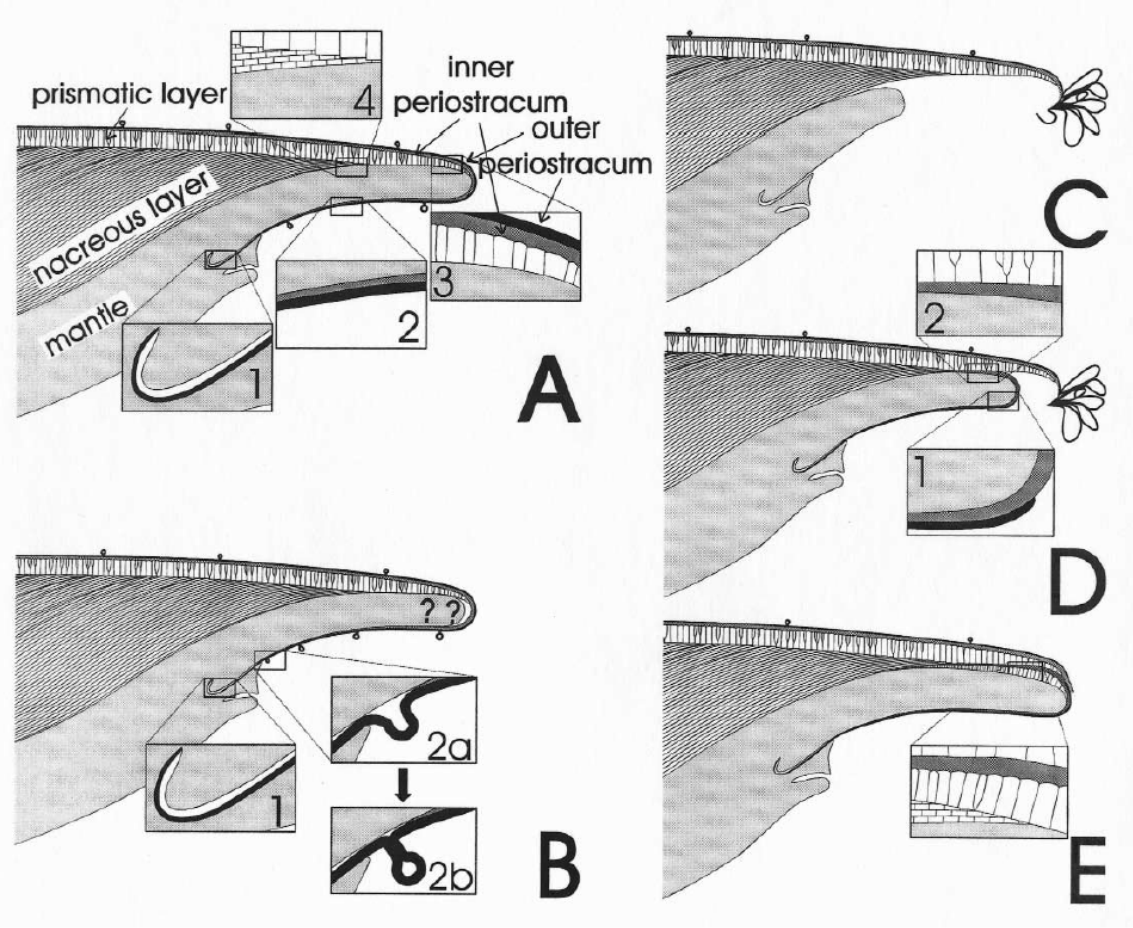

Fig. 3.1: Model proposed by A.Checa [16] for the formation of the periostracum and shell in Unionidae.

outer mangle fold is fully extended, calcification proceeds on the inner periostracal layer (inset).

Since bivalves are sensitive organisms, it is assumed that environmental changes could affect the texture of their shells. Study focused on the effect of salinity and pH treatments on the crystal orientation in mussel shells was done in [11]. They showed that biomineralization processes are disturbed by lower pH environments, where salinity plays minor role. Another study that tried to study the effects of many elements (total of 24) present in the shell by means of neutron activation analysis (NAA) [12]. This method is proficient at determination of specific group of elements considered as markers - key elements, which allow for estimation of the significance of terrigenous and anthropogenic factors. They were able to measure values of Mn, Ni, Zn and As - known to indicate pollution and distinguish polluted areas from non-polluted by the observation of the molluscs. They were also able to link the presence of some elements in higher amounts to the stress environments for the mussels. Most important finding of the study correlating with this work is, that the crystallographic textures of mussel shells from the studied bays showed insignificant dissimilarities despite despite significant differences between concentrations of

elements among chosen bays.

Main building material of molluscan shell is calcium carbanate $CaCO_3$, forming crystals of calcite, aragonite and rarely vaterite. Parts are formed with small amount of other organic substances. The molecular workings of formation, shaping and orientation of individual $CaCO_3$ crystals is largely complex and still not well understood despite being intensively studied for the last four decades [14,15]. The carbonate mono or polycrystals composing the shell form many different microstructures and textures. Several experiments have already shown that the style of nanoscale organization of inorganic and organic components of the molluscan shells considerably changes their properties. Understanding of the biomineralization process on a molecular level should improve the preparation of new nanocomposites.
As each particular shell microstructure is complex nanocomposite which is also product of very complex structural mechanism, development of shell layer with same microstructure and texture is highly unlikely. Better understanding of the microstructure and texture of individual shell layers will provide new data source for understanding the long evolution of molluscs. Extremly rich and diverse fossil record of molluscan evolution gives the chance to study many inorganic biomineralization product. Shell microstructure characterizing the shape of biocrystals, has been the most studied property of molluscan shells. On the other hand, there are very lattle data concerning crystallographic texture that describes the arrangement of crystal axes of individual biocrystals (providing us with non-redundant characteristics of a particular shell layer). In this thesis we present the crystallographic texture analysis of nacre in Bivalve shell *Sinanodonta woodiana*.

3.1.1 Sinanodonta woodiana

Sinanodonta woodiana bolongs to species of East Asian unionid mussel. They are able to reproduce in their first year of being with only 4 cm sizes. They reach up to large 30 cm, in age of 12-14 years. They are invasive freshwater rivel mussels of the class Bivalvia, order of Unionida and family Unionidae. These important parasitic species are not native to Czech Republic rivers, but they are present since 1996. Great success of *Sinanodonta woodiana* is attributed to importation and commercialization od Asian carp, its native host. Our samples were collected by Czech University of Life Sciences Prague in river Lužnice. Samples of *Sinanodonta woodiana* were collected dead so no harm was done to the individual molluscs.

3.2 Phase analysis

A X-ray and neutron phase analysis was performed on the samples with diffractometers SmartLab Rigaku (with CuK_α rotating anode) located at the Institute of Physics of the Academy of Sciences of the Czech republic and KSN-2 (described in previous chapters). Chosen specimen of *Sinanodonta woodiana* was grinded into a smooth powder. Data from X-ray diffractometer were processed in software HighScore plus

while using entries from database PDF-4. Data from KSN-2 were processed in GSAS-II [19]. Results from X-ray and neutron phase analyses were in agreement and show that species *Sinanodonta woodiana* consist of only a single phase, that of aragonite 3.2. This leads to simplified crystallographic texture analysis. In the figure 3.2 it is possible to also see the crystallographic planes of aragonite responding to reflections. Aragonite as an carbonate mineral crystallizes in an orthorhombic crystal system. Aragonite may be columnar or fibrous and repeating twinning in aragonite causes iit to turn into pseudo-hexagonal forms. It's lattice parameters consists of three 90° angles and sides of dimensions $a = 4.95$ Å, $b = 7.96$ Åand $c = 5.74$ Å. Space group of aragonite is *Pmcn*.

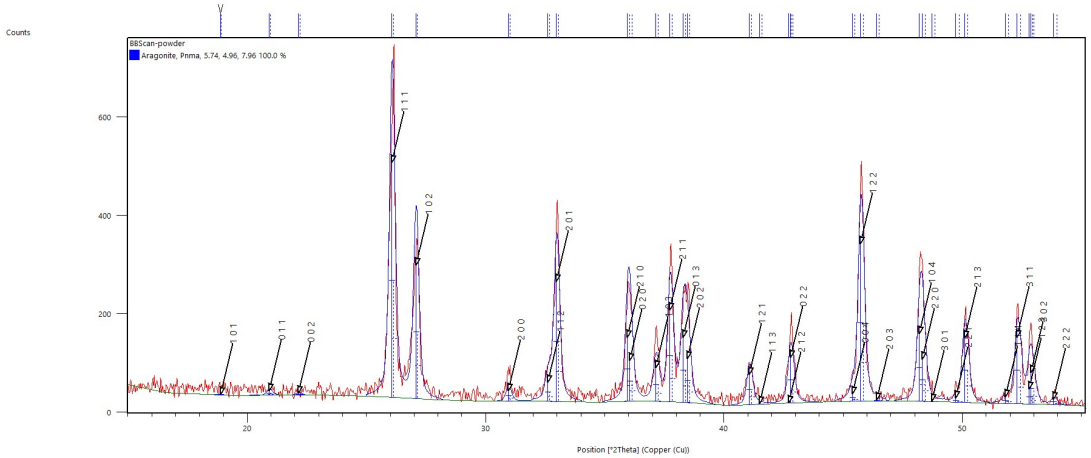

Fig. 3.2: X-ray phase analysis of *Sinanodonta woodiana* inner nacreous shell.

3.3 Texture analysis

The shell part analyzed by an X-ray diffraction was nacreous layer of inner shell. From previous studies it became clear that texture strength is different for the young specimen and adult bivalve [20]., thus shaping a similar question, whether the texture changes also in relation to direction of growth illustrated in 3.4. Sample was divided into 4 approximately square parts as show in figures 3.3, 3.4 and those were studied on X-ray diffractometer individually.

The X-ray pole figures were measured until the tilt became $\varphi = 70°$. Pole figures were measured for planes with Miller indexes: (111) ,(102),(200),(201) and (002). For handling the texture data X-ray diffraction data application SmartLabStudio II from Rigaku was used. By employing WIMW method that was declared in 1.3, the orientation distribution function was computed. Prerequisites for determining the remaining 20 degrees of angle φ were accomplished by computing ODF. From this point, it was possible to compute all other pole figures of crystallographic planes, particularly for the significant planes (100), (010) and (001).

Fig. 3.3: Sample used for X-ray diffractometer in comparison to human hand.

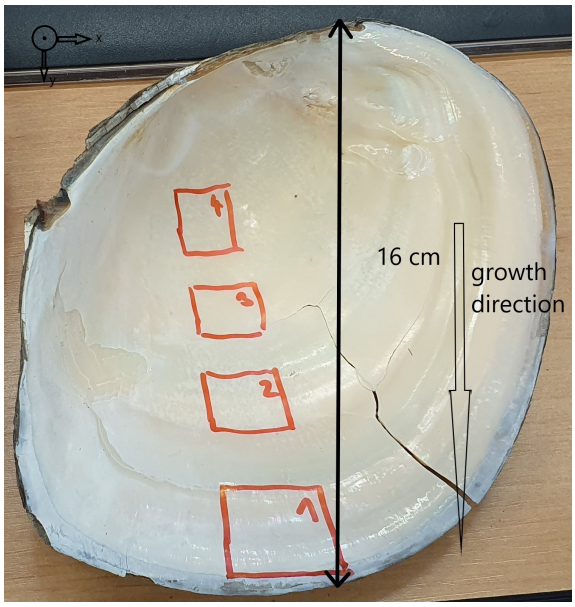

Fig. 3.4: Sample with marked growth direction and square parts illustrated.

Neutron pole figures were measured for planes (002) that can be directly compared to (001) and (102). Neutronographic data was analyzed by software GSAS-II [19].

3.4 Results

X-ray phase analysis is shown in figure 3.2. The phase analysis of the shell confirms that *Sinanodonta woodiana* is made up of only aragonite. Complete neutron pole

figures measured for planes (102) and (002) are depicted in 3.5. Calculated X-ray pole figures of surface nacreous layer for planes (100), (010) and (001) are shown in figure 3.7. Figure 3.6 shows ODF sections at $\Phi = 90°$.

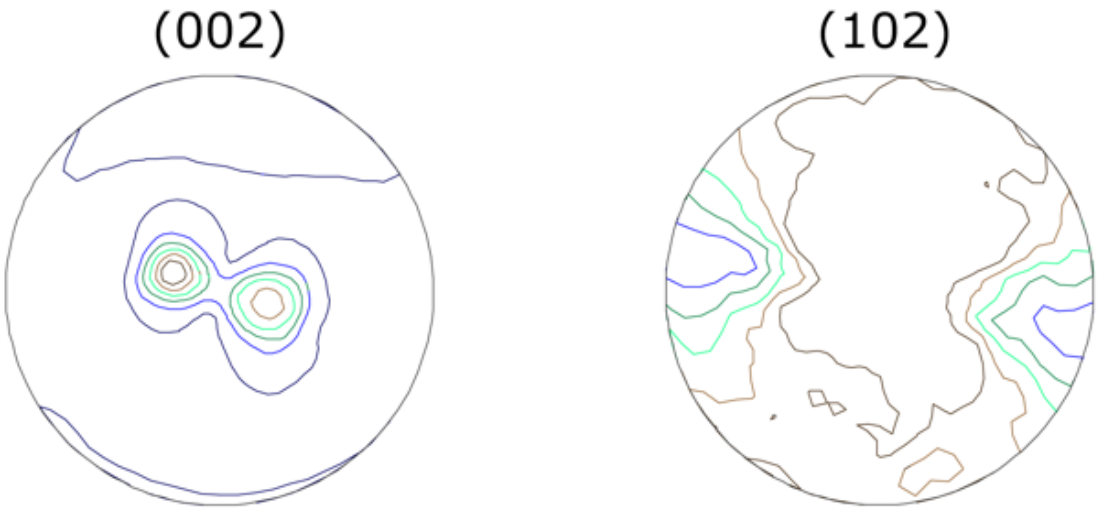

Fig. 3.5: Complete neutron pole figures for planes (102) and (002) for the mollusc sample *Sinanodonta woodiana* measured on diffractometer KSN-2.

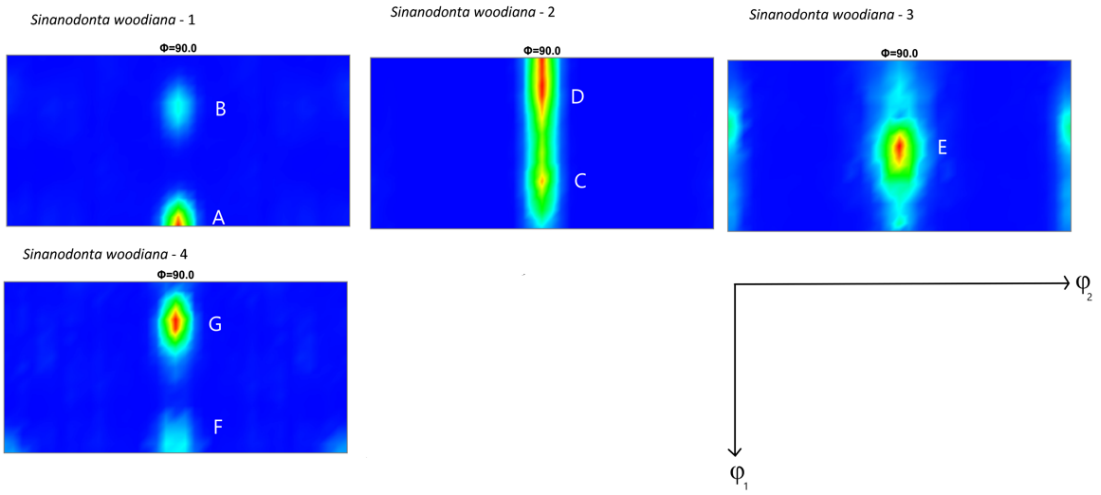

Fig. 3.6: ODF sections ($\Phi = 90°$) calculated from X-ray pole figures for *Sinanodonta woodiana*. There are four investigated areas 1-4 responding to cut out squares of the sample.

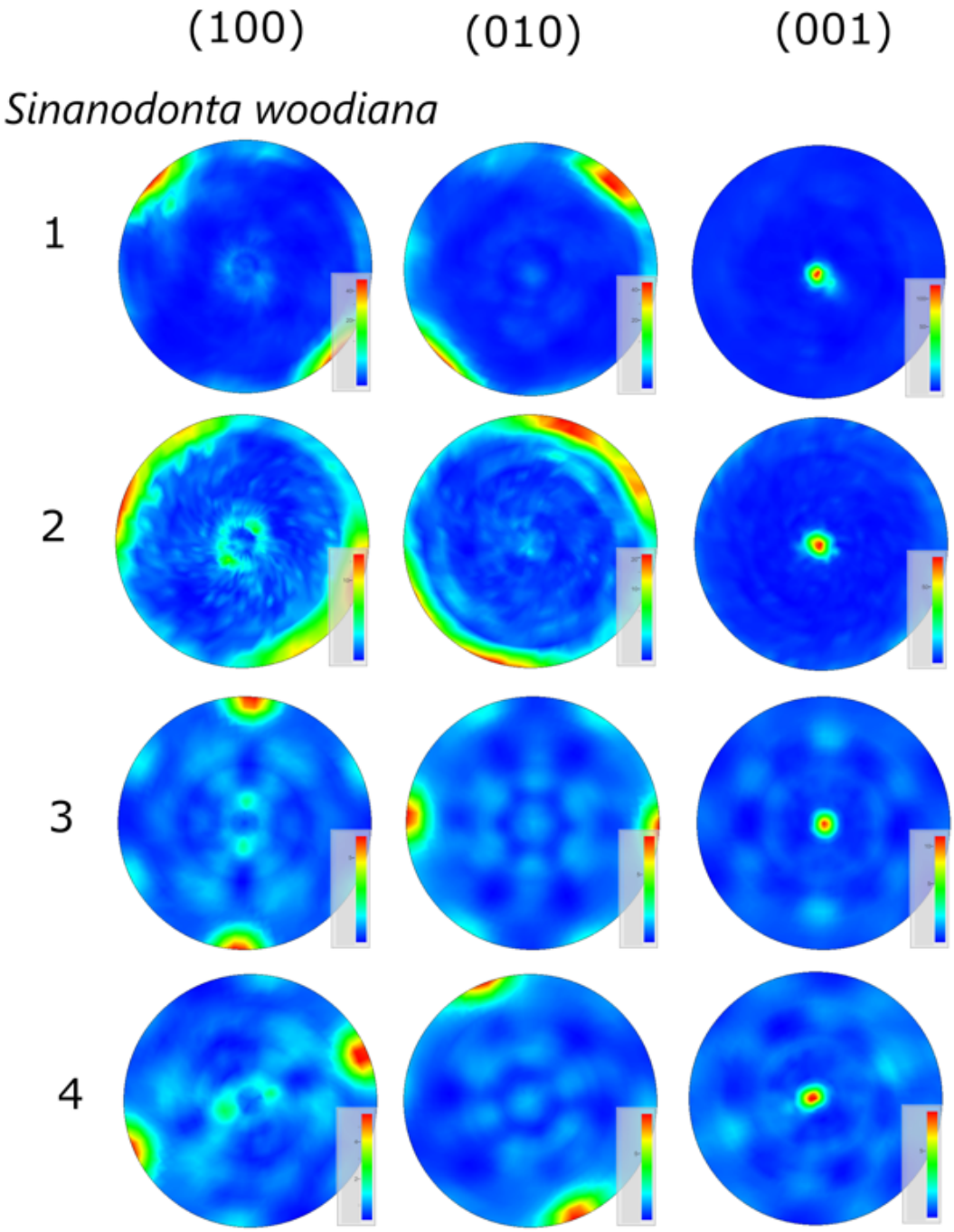

Fig. 3.7: Complete X-ray pole figures for planes [100],[010] and [001] for the mollusc sample *Sinanodonta woodiana* calculated from X-ray diffraction data.

3.5 Discussion and conclusions

In the previous studies [17,18] there was a conclusion that c-axis of aragonite grains - crystallographic direction <001> is preferentially orientated perpendicular to the inner shell surface in all studied bivalve species. It follows from both X-ray and neutron diffraction pole figures shown in figures 3.5, 3.7 that data we measured are

in agreement with this statement. The preferential orientation of crystallites is indicated by a sharp maximum in the center of [001] pole figures. By comparing pole figures from different parts of the shell, it is evident that the maximum widens slowly along the growth direction (from 1 to 4). It can be interpretated as slight deviation from the ideal pure fiber texture along the opposite of a growth direction, therefore shell's nacre tends to have more preferentially oriented c-axis parallel to the surface at the edges of the shell. This result is in agreement with neutron diffraction pole figures describing global texture data, which show similar global texture maxima and confirming slight deviation from the ideal fiber texture.

Next observation that can be made is of rotation of b and a axes. Growth direction on the pole figures is to the right of the center. Observing the b-axis in pole figures (010) of square piece 1, we see that the axis is tilted to the side of the growing direction. Progressing in pole figure of square piece 3 to being parallel to growth direction, the b-axis made a movement, a change of preferred orientation. In the last piece b-axis continues rotating clockwise to being almost parallel to the growth direction. Same effect is visible on axis a, but in opposite phase.

When assessing the texture strength, we can use the pole maximum value in (001) pole figures in place of characteristics. Study of this parameter leads to observation that there is strong growing tendency in the opposite direction to the growth direction. In square no. 4 the maximum value amount to ca. 5 m.r.s. In square no. 1 the texture strength grows to the 100 m.r.s. That means texture strength increases 20-fold along the negative growth direction.

Bibliography

[1] K.H.BECKURTS and K.WIRTZ *Neutron physics*. Heidelberg Springer-Verlag Berlin 1964, p. 3 ISBN:978-3-642-87616-5

[2] JOHN R.LAMARSH and ANTHONY J.BARATTA *Introduction to Nuclear Engineering - Third edition*. Prentice Hall Upper Saddle River, New Jersey ISBN 0-201-82498-1

[3] MONIKA KUČERÁKOVÁ *Disertační práce: Studium textur polykrystalických materiálů pomocí rentgenové a neutronové difrakce*. Czech technical university in Prague, Faculty of Nuclear Sciences and Physical Engineering- Prague 2015

[4] G.E.BACON *Neutron Diffraction*. Oxford, Clarendon Press, 3rd edition, 1975.

[5] Z.SMETANA, V.ŠÍMA *Neutronová difrakce - Vyd.1.*. Praha: Matematicko-fyzikální fakulta UK, 1982,. Experimentální metody fyziky pevných látek, sv. 5. p. 99

[6] C. Z. CHRISTENSEN, A. NIELSEN, A. BAHNSEN, W. K. BROWN, B. M. RUSTAD *Free-Neutron Beta-Decay Half-Life*. Danish Atomic Energy Commission, Research Establishment Riso, Physics DePartment, Roskilde, Denmark 1972

[7] ING. JIŘÍ ČAPEK, PH.D *Textura*. Presentation 2020/2021

[8] I.KRAUS, J.FIALA *Krystalografie* Česká technika - nakladatelství ČVUT Praha 2021

[9] U.F.KOCKS, C.N.TOME, H.-R. WENK *Texture and anisotropy: preferred orientations in polycrystals and their effect on materials properties* Cambridge university press, 1998, 677 s. ISBN 0-521-46516-8.

[10] MATTHIES, S., H.-R. WENK a G. W. VINEL *Some basic concepts of texture analysis and comparison of three methods to calculate orientation distributions from pole figures*Journal of Applied Crystallography 1988 doi:10.1107/S0021889888000275

[11] C.GRANIER, R. ROMÁN, C.DUERTE, J.M. NAVARRO, A.B. RODRIGUEZ-NAVARRO, L. RAMAJO *The combined effects of salinity and pH on shell biomineralization of the edible mussel Mytilus chilensis* Environ. Pollut 2020, 263, 114555

[12] P.NEKHOROSHKOV,I. ZINICOVSCAIA, D. NIKOLAYEV, T. LYCHAGINA, A. PAKHNEVICH, N. YUSHIN, J. BEZUIDENHOUT *Effect of the Elemental Content of Shells of the Bivalve Mollusks (Mytilus galloprovincialis) from Saldanha Bay (South Africa) on Their Crystallographic Texture* Biology 2021, ISSN 2079-7737

[13] B.KRATOCHVÍL *Chemie a fyzika pevných látek I.* 2nd ed. Praha : VŠCHT Praha, 1994. ISBN 80-7080-196-4

[14] F.MARIN, G. LUQUET, B. MARIE, D. MEDAKOVIC *Molluscan Shell Proteins: Primary sructure, Origin, and evolution* Current Topics in Developmental Biology 2008

[15] M.SUZUKI, K.SARUWATARI, T. KOGURE, Y.YAMAMOTO, T. NISHIMURA, T.KATO, H.NAGASAWA *An acidic Matrix Protein,PiF, Is a Key Macromolecule for Nacre Formation* Science 325 , 2009

[16] A. CHECA *A new model for periostracum and shell formation in Unionidae (Bivalvia, Mollusca)* Tissue and Cell 2000 ISSN 00408166

[17] FRÝDA, J., K. KLICNAROVÁ, B. FRÝDOVÁ a M. MERGL *Variability in the crystallographic texture of bivalve nacre* Bulletin of Geosciences 2010 ISSN 1802-8225

[18] D.CHATEIGNER, C.HEDEGAARD, H.-R. WENK *Mollusc shell microstructures and crystallographic textures* Journal of Structural Geology 2000 DOI 10.1098/S0191-8141(00)00088-2

[19] B.H.TOBY *EXPGUI, a graphical user interface for GSAS* J.Appl.Crystallogr. 2001 https://doi.org/10.1107/S0021889801002242

[20] KUCERAKOVA, M., J. ROHLICEK, S. VRATISLAV, D. NIKOLAYEV, T. LYCHAGINA, L. KALVODA a K. DOUDA *Texture Study of Sinanodonta Woodiana Shells by X-Ray Diffraction* Journal of Surface Investigation: X-ray, Synchrotron and Neutron Techniques, 2021 ISSN 1027-4510

[21] H.J.BUNGE *Texture Analysis in Materials Science* 1982 DOI:10.13140/RG.2.1.1721.1041

Appendixes can be found in the documents attached to the thesis.

/1/ Ampl_Rozpt_b.doc
/2/ Ampl_b1
/3/ binding_energy